The Nansen Environmental and Remote Sensing Center

NERSC

A non-profit environmental research institute affiliated with the University of Bergen

Edvard Griegsvei 3a, N–5037 Solheimsvik, Norway

Technical Report No. 54

A Feasibility Study of Dissolution and Sequestration of CO_2 in the Ocean

Final report of a project executed by NERSC for Statoil

Helge Drange & Peter M. Haugan

17 March 1992

Technical Report No. 54

A Feasibility Study of Dissolution and Sequestration of CO_2 in the Ocean

Executive Summary

The uptake of anthropogenic CO_2 across the air-sea interface is slow and a considerable transient increase in atmospheric CO_2 content is expected in the next century and beyond. Successful injection of CO_2 in the ocean will reduce or remove the expected transient maximum in atmospheric CO_2 concentrations compared to the case of continued emissions to the atmosphere. Injection is not equivalent to reduced total burning, but it will reduce the maximum perturbation of the climate system and thereby reduce the probability of large climate changes.

In order to obtain successful sequestration in the deep ocean, injection at large depths or in sinking currents has been proposed. We demonstrate in this study that also injection at shallow depths (200 - 400 m) may work well. The increase in seawater density due to dissolved CO_2 is significant and will contribute to sinking of CO_2-enriched water.

Shallow injection may be carried out by dissolving CO_2 in seawater at elevated pressure and pumping the enriched water to the release depth. We demonstrate in this study that direct pumping of gaseous CO_2 into the ocean may also work well. In either case, the release point should ideally be located near a sloping bottom which can lead the enriched water to great depths with minimum dilution from ambient water.

Several locations relatively close to the coast of Norway should be well suited for injection leading to long term sequestration in the deep ocean.

Before injection in the ocean can be recommended, the theoretical predictions presented here should be verified by more detailed studies, and possible environmental damage near the injection point should be investigated. However, the results of this study certainly indicate that injection at 200-400m depth near the coast may be efficent for long term sequestration in the ocean.

Bergen, 17/3 1992

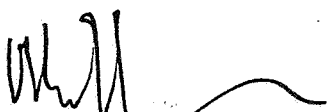

O. M. Johannessen
Director

Nansen Environmental and Remote Sensing Center
Edvard Griegsvei 3A,
N-5037 SOLHEIMSVIK,
NORWAY.
Phone: +47 5 29 72 88
Fax - 47 5 20 00 50

Contents

List of Figures

List of Tables

A Feasibility Study of Dissolution and Sequestration of CO_2 in the Ocean

1 Introduction

This report describes the results of a research project carried out by NERSC for Statoil in the period November 1991 through January 1992. We focus on the chemical and physical interactions which are expected to take place when CO_2 meets seawater, and the fate of injected carbon on a short (less than a day) and long (more than 100 year) time scale. Technical and economical aspects of various modes of injection are not included in the study. Emphasis is put on options which are thought to be attractive from a technical and economical point of view, i.e. near shore or shallow water injection.

Some of the most important previous studies of CO_2 injection are reviewed in Section 2. Global scale studies of the expected future atmospheric CO_2 levels when parts of the expected CO_2 emissions are injected in the ocean, as well as detailed studies of dissolution of injected drops of liquid CO_2 are discussed. Appendix A contains further discussion of the buffering of atmospheric CO_2 in the oceanic surface layer (order 1 - 2 years) and the long term (order 1000 year) partitioning of CO_2 between the atmosphere, the ocean and the bottom sediments.

In Section 3 the relevant chemical properties of CO_2 in seawater are studied. A rather complete account is given of the phase behaviour and solubility based on data from various sources. An important result is the increase in seawater density due to dissolution of CO_2, which may make shallow injection more attractive than what has been previously assumed.

This leads to Section 4 where the process of dissolution of CO_2 from bubbles released into seawater is studied in some detail. Bubble flow regimes and break-up processes are discussed. A numerical model has been developed and is used to study the speed of dissolution from rising bubbles released at various depths.

In Section 5 outgassing back to the atmosphere is demonstrated to be rapid if injection takes place in such a way that the injected carbon is not kept away from the ocean surface. Small scale mixing processes that would dilute a plume containing injected CO_2 are briefly discussed. With this and the previous results in mind, we give a brief discussion of possible application of CO_2 injection along the coast of Norway.

The conclusions in Section 6 include recommendations for further work.

2 Previous CO_2 Injection Studies

In this section we review and present the most important findings from the existing ocean disposal literature. Some of the results — the estimated steady-state value of atmospheric CO_2 after the period with fossil fuel burning and the effect of CO_2 disposal on the oceanic uptake of atmospheric CO_2 — are discussed in Appendix A.

2.1 The Marchetti Scenario

The ocean plays an important role in the global carbon cycle, and the oceanic waters and sediments have capacity to neutralize the amount of carbon locked up in the known, recoverable fossil fuel reserves (Broecker and Peng, 1982). However, the oceanic uptake of anthropogenic, atmospheric CO_2 is slow — thousands of years are required before equilibrium between the atmosphere, ocean and sediments is achieved. The reason for the slow overturning of atmospheric CO_2 in the ocean is partly found in the slow uptake of CO_2 through the mixed upper layer of the ocean, and partly in the low rate of mixing between the deep waters and surface waters. It was therefore proposed by Marchetti, 1977, to collect and compress CO_2 from coal, oil and gas power plants, and to pipe and inject it directly into the ocean. Marchetti identified the Strait of Gibraltar as a promising place; here the saline and heavy outflowing Mediterranean water sinks, and would therefore spread and dilute the CO_2 over practically all the Atlantic. As other possible injection places, Marchetti mentions the Weddell Sea and the Norwegian Sea, regions where deep water is formed.

The paper by Marchetti was followed by Mustacchi *et al.*, 1979, who reviewed various options for removing CO_2 from power plant exhaust gases, and Hoffert *et al.*, 1979, who used a simple marine carbon cycle model and looked at the atmospheric response of oceanic CO_2 disposal. Results from the latter paper are shown in Fig. 1. The model calculations are based on emission rates which are more than extreme, but the results are interesting, important and clearly show the effect of oceanic CO_2 injection: By injecting CO_2 into the ocean, one can reduce or prevent the transient but not the final steady-state value of atmospheric CO_2 concentration.

The very high maximum atmospheric concentration in Fig. 1 is due to the high emission rates. The pCO_2 is probably overestimated in the cases where large parts of the CO_2 are emitted directly to the atmosphere also because the model does not properly include the fast pathways to the deep ocean through deep water formation (Siegenthaler, 1983). The final atmospheric CO_2 concentration is about 1150 ppm, which is 4.1 times the preindustrial atmospheric value. The model does not include the effect associated with dissolution of sediments; including the sediments would lead to a final atmospheric value of about 575 ppm. The same final atmospheric concentration would be obtained if the same amount of fossil fuels were burned over a much longer period of time. The model does not take into account the terrestrial biosphere, potential changes of the marine biota, or feedback mechanisms from change in the climate system.

2.2 Some Deep Ocean Disposal Options

Possible deep ocean disposal options for CO_2 are discussed by Baes *et al.*, 1980. The most realistic options are found to be

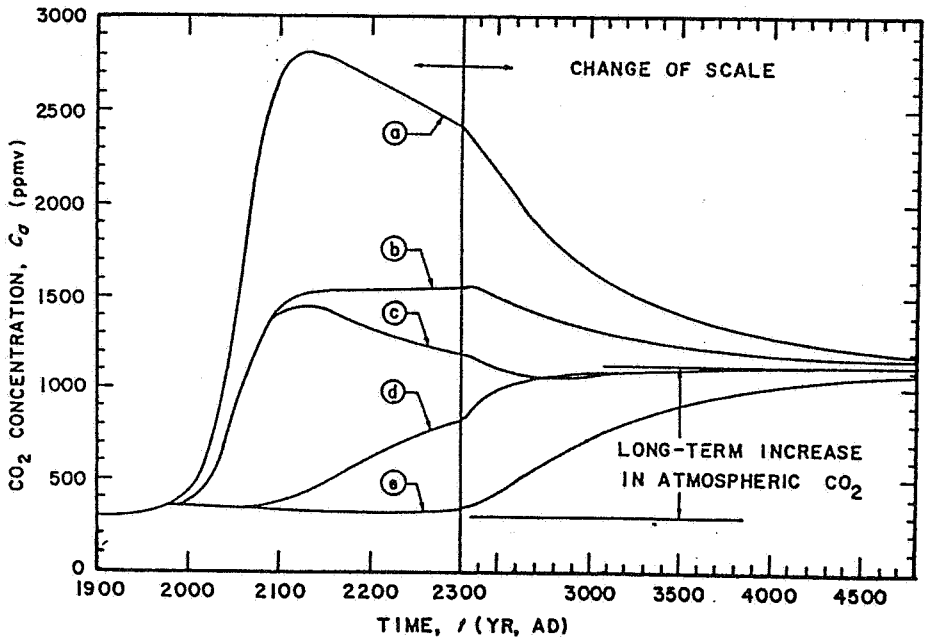

Figure 1: Atmospheric CO_2 concentration assuming the entire fossil fuel reserve of 7×10^3 Gt C is burned. (a) 100% of the released CO_2 is injected into the atmosphere, (b) 50% injected at oceanic depth of 1500 m and 50% into atmosphere, (c) 50% injected at sea floor and 50% injected into atmosphere, (d) 100% injected at oceanic depth of 1500 m, and (e) 100% injected at sea floor. Figure from Hoffert *et al.*, 1979.

i) To produce and inject negatively-buoyant plumes of highly CO_2-enriched seawater at depths greater than 500 metres

ii) To pipe and release liquid CO_2 at depths greater than 3000 metres, where liquid CO_2 is heavier than the surrounding water

iii) To form and drop blocks of dry ice or solid carbon dioxide hydrate with a density greater than that of seawater

iv) To inject CO_2 into depleted oil and gas fields

Of these options, Baes *et al.*, identified option i) as the preferred one, and option ii) – iv) as possible.

Baes *et al.* have studied option i) in some detail. Since CO_2-enriched seawater is heavier than ambient seawater (Subsec. 3.9), this fluid tends to sink in the ocean. In order to prevent bubble formation, the authors recommend an injection depth greater than about 500 metres. The heavy fluid can be produced by dissolving compressed CO_2 gas in seawater. The behaviour of the negatively-buoyant plumes are studied by use of an analytical model developed by Lee, 1980.

Herzog *et al.*, 1991, consider dissolution rates of liquid CO_2 drops released at depths between 500 and 2000 metres. At these depths, liquid CO_2 is lighter than seawater (Subsec. 3.2), and the CO_2 drops will rise. To ensure that the CO_2 drops are completely dissolved at a depth of about 500 metres — where CO_2 is in the gaseous phase — they found that the liquid CO_2 should be released at depths greater than 700 metres. Herzog *et al.* stress the importance of a diffusor at the injection site such that the initial drop radii are less than 1 cm. From estimates of the largest stable drop radius as a function of depth given in the paper by Herzog *et al.*, we conclude to the contrary that no diffusor will be needed, since large drops are expected to break-up. We also find that dissolution above the depth of phase transition will be sufficiently rapid to avoid direct outgassing of the injected CO_2 (Sec. 4).

2.3 Ocean Disposal Studies with the Hamburg Model

Recently, a global ocean circulation and marine carbon cycle model developed in Hamburg (Maier-Reimer and Hasselmann, 1987; Maier-Reimer and Bacastow, 1990; Heinze *et al.*, 1990; and Bacastow and Maier-Reimer, 1991) has been used to investigate the feasibility of CO_2 sequestration in the ocean. In contrast to the model used by Hoffert *et al.*, the Hamburg-model treats the ocean as a dynamic system. This model definitely represents state-of-art within large scale carbon cycle modelling.

With the Hamburg model, Bacastow and Stegen, 1991; and Stegen *et al.*, 1991, have considered the increase in atmospheric CO_2 from a 1 GW coal-fired power plant operating for 100 years, starting from an atmospheric CO_2 concentration of 282 ppm. The injection has been taken in the North Pacific, and several scenarios are run. Fig. 2 summarizes the results. As we see, ocean disposal of CO_2 decreases the transient value of atmospheric CO_2 concentration. The success of the injection, i.e. the number of years the injected CO_2 remains in the ocean, depends on the ocean currents and the mixing in the actual region. Since the physics of the North Pacific is characterized by upwelling and rather strong vertical mixing, this region is not favourable for CO_2 injection. As in the work of Hoffert *et al.*, the final atmospheric equilibrium level is the same for all the scenarios. Bacastow and Stegen, 1991,

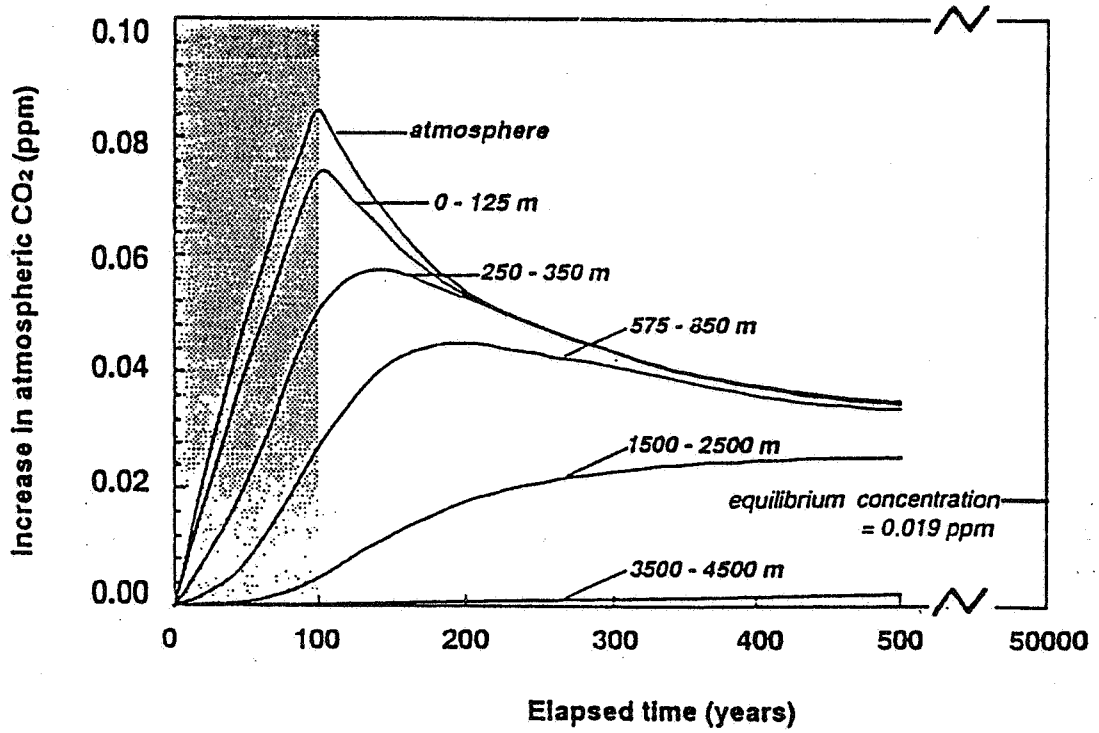

Figure 2: The increase in atmospheric concentration of CO_2 from a 1 GW coal power plant operating for 100 years (the hatched region). The curves give the increase if all of the CO_2 is released into the atmosphere, or in the ocean at the depths indicated. Figure from Stegen *et al.*, 1991.

and Stegen *et al.*, 1991, found that about 12% of the released CO_2 ultimately end in the atmosphere.

The Marchetti scenario has been studied by Maier-Reimer, 1991. Starting in 1989, one third of the worlds expected total CO_2 emissions was released in the deep water off the Spanish coast. In comparison, a control experiment without the ocean disposal was also run. In the year 2100, the injection experiment predicts an increase in atmospheric CO_2 concentration slightly less than two thirds of the increase in the control run (this result is discussed in some detail in Subsec. A.3). This study demonstrates the capacity of the ocean to handle large amounts of CO_2 on a 100-year time scale.

2.4 Summary

Little theoretical work has been done on the feasibility of oceanic disposal of CO_2, and we are not aware of any work on the possibility of shallow CO_2 injection in the ocean. The studies with the Hamburg model show, however, the oceanic capacity to handle large amounts of CO_2, and to reduce the transient pCO_2 maximum. The latter point is also shown in a box-model study (Hoffert *et al.*, 1979).

3 CO_2 in Seawater

In this section we give a short review of the carbon chemistry in seawater, and discuss the properties of different forms of CO_2 and CO_2-enriched fluids. The main goal is to determine the CO_2 uptake capacity of seawater, and the corresponding increase in seawater density.

3.1 Carbon Chemistry in Seawater

For a general discussion of the inorganic chemistry in seawater, see Riley and Skirrow, 1975; and Stumm and Morgan, 1981.

The relationships between the different chemical species of the carbonic acid system in seawater can be represented by the reactions (Stumm and Morgan, 1981):

$$CO_2(aq) + H_2O \overset{K'}{\rightleftharpoons} H_2CO_3\,, \tag{1}$$

$$H_2CO_3 \overset{K'_*}{\rightleftharpoons} HCO_3^- + H^+\,, \tag{2}$$

$$CO_2(aq) + H_2O \overset{K'_1}{\rightleftharpoons} HCO_3^- + H^+\,, \tag{3}$$

$$HCO_3^- \overset{K'_2}{\rightleftharpoons} CO_3^{2-} + H^+\,. \tag{4}$$

Here the K''s are the apparent equilibrium constants for the reactions, and $CO_2(aq)$ is dissolved carbon dioxide, H_2CO_3 carbonic acid, HCO_3^- bicarbonate ion and CO_3^{2-} carbonate ion. For seawater there are two main hydration paths; reaction (1) and (3). As we shall see, most of the non-ionized carbon dioxide ($CO_2(aq)$ and H_2CO_3) is present in the form $CO_2(aq)$. It is therefore usual to include both the hydration reaction and the protolysis of H_2CO_3 in K'_1. The hydration and protolysis for the carbonic system are then given by reaction (3) and (4). K'_1, including H_2CO_3, is known to a high degree of accuracy. The equilibrium constants depend on temperature, salinity and pressure, and analytical expressions are given in UNESCO, 1987.

In the following, $[i]$ denotes number of moles per volume, or concentration, of species i. The volume is taken as m^3, or for convenience, as litre $L = 10^{-3}\ m^3$. The total concentration of inorganic carbon C_T is defined as

$$C_T = [CO_2(aq)] + [H_2CO_3] + [HCO_3^-] + [CO_3^{2-}]\,. \tag{5}$$

The concentration of H^+-ions is usually expressed in terms of the pH value defined as

$$pH = -\log[H^+]\,. \tag{6}$$

Another important quantity is the alkalinity A, which may be approximated by the following expression (e.g. Butler, 1982):

$$A = [HCO_3^-] + 2[CO_3^{2-}] + [B(OH)_4^-] + [OH^-] - [H^+]\,. \tag{7}$$

The unit of the alkalinity quantity is equivalents per volume, or number of moles of charges per volume.

In Eq. 7, $[B(OH)_4^-]$ represents the borate system in seawater. The borate system is given by the first dissociation of boric acid:

$$B(OH)_3 + H_2O \overset{K'_B}{\rightleftharpoons} B(OH)_4^- + H^+\,. \tag{8}$$

The total concentration of borate,

$$B_T = [B(OH)_3] + [B(OH)_4^-]. \tag{9}$$

B_T is reported to be proportional to salinity S (Culcin, 1965), and

$$B_T = (S/35) \cdot 4.106 \times 10^{-4}. \tag{10}$$

The OH^-- and H^+-ions in the above reactions are connected through the dissociation reaction of water

$$H_2O \overset{K'_w}{\rightleftharpoons} H^+ + OH^-. \tag{11}$$

Analytical expressions for the apparent equilibrium constants K'_B and K'_w as functions of temperature, salinity and pressure are given in UNESCO, 1987.

One important property of the alkalinity is that it does not change when CO_2 is added or withdrawn from the solution (Stumm and Morgan, 1981). This is so because alkalinity measures the proton deficiency with respect to the reference proton level of pure CO_2 and water. Or put another way; addition or removal of CO_2 does not affect the net charge balance of the solution.

There are, of course, reactions and processes that do affect the alkalinity. The most important reaction here is the dissolution/formation of calcium carbonate sediments (Stumm and Morgan, 1981; Broecker and Peng, 1982). A short discussion of the dissolution of calcium carbonate sediments is given in Subsec. A.2.

Reactions 1, 3 and 4 can be illustrated graphically in a logarithmic concentration diagram, see Fig. 3. In this figure we have plotted the concentrations of $[H_2CO_3]$, $[CO_2(aq)]$, $[HCO_3^-]$ and $[CO_3^{2-}]$, all normalized to C_T, as functions of $[H^+]$. From the figure, we see that for pH ≈ 8.2 (corresponding to 'normal' seawater), the carbonic system is given by approximately 92% $[HCO_3^-]$, 7% $[CO_3^{2-}]$, 1% $[CO_2(aq)]$, and almost no $[H_2CO_3]$.

In Fig. 4, we have plotted the concentrations of the carbonic species and H^+-ions as functions of C_T. The starting value of C_T, $C_T = 2.2$ moles m^{-3}, is a typical value for todays ocean. For increasing C_T concentration, for instance by adding $CO_2(aq)$ to seawater, the pH value decreases; the water becomes more acid. For $C_T \gtrsim 3.5$ moles m^{-3}, which may easily be obtained by artificial addition of CO_2 to seawater, the variations in C_T are well approximated by variations in $[CO_2(aq)] + [H_2CO_3]$. One can therefore neglect carbon chemistry associated with the dissociation reactions of carbonic acid for $C_T \gtrsim 3.5$ moles m^{-3}. The carbon system is then given by $[CO_2(aq)] + [H_2CO_3] \approx [CO_2(aq)]$, and approximately constant $[HCO_3^-]$.

3.2 Gaseous, Liquid and Hydrate CO_2

The condensation line for pure CO_2 is shown in Fig. 5. The condensation pressure P_{cond} (bar) depends on the temperature according to the second order polynomial

$$P_{\text{cond}}(T_c) = 34.8649 + 0.90485 \cdot T_c + 0.0108504 \cdot T_c^2 \tag{12}$$

for $-1.7 < T_c < 20°C$. The gaseous phase is therefore the stable phase for pressures below the line in Fig. 5, and the liquid phase is the stable phase above the line.

The density of liquid CO_2 is shown in Fig. 6 as a function of pressure and temperature. As we see, liquid CO_2 is lighter than seawater in the uppermost 3000 metres of the ocean,

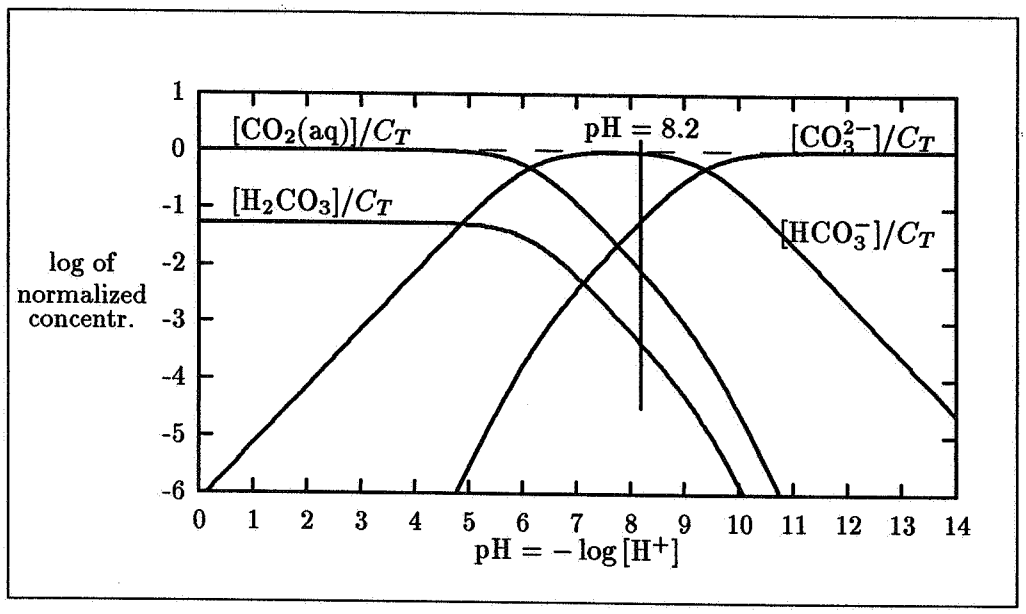

Figure 3: Logarithmic concentration diagram showing the ratios of carbonate species to total inorganic carbon as a function of pH. The values of the apparent equilibrium constants (taken from UNESCO, 1987), correspond to surface seawater with 35 pro mil salinity and temperature of 5°C. The vertical line indicates the pH value of normal seawater.

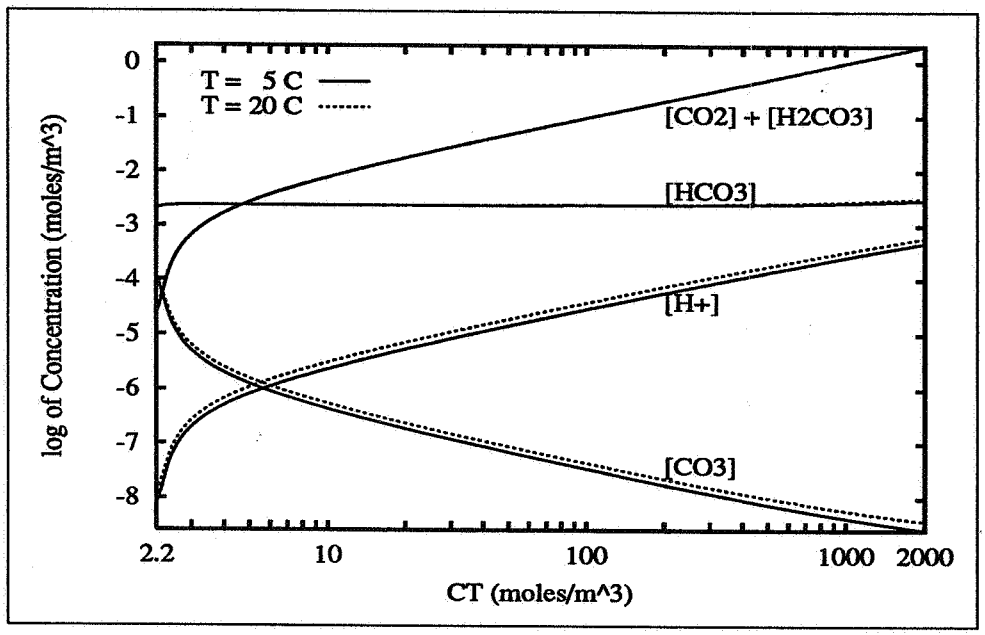

Figure 4: Concentration of carbonic species and H^+-ions as functions of C_T. The plot is based on apparent equilibrium constants (UNESCO, 1987) for 35 pro mil salinity, $P = 30$ bar, and temperatures as indicated. The alkalinity A is set to 2.35 equiv m^{-3}. The borate system has been included in the computations.

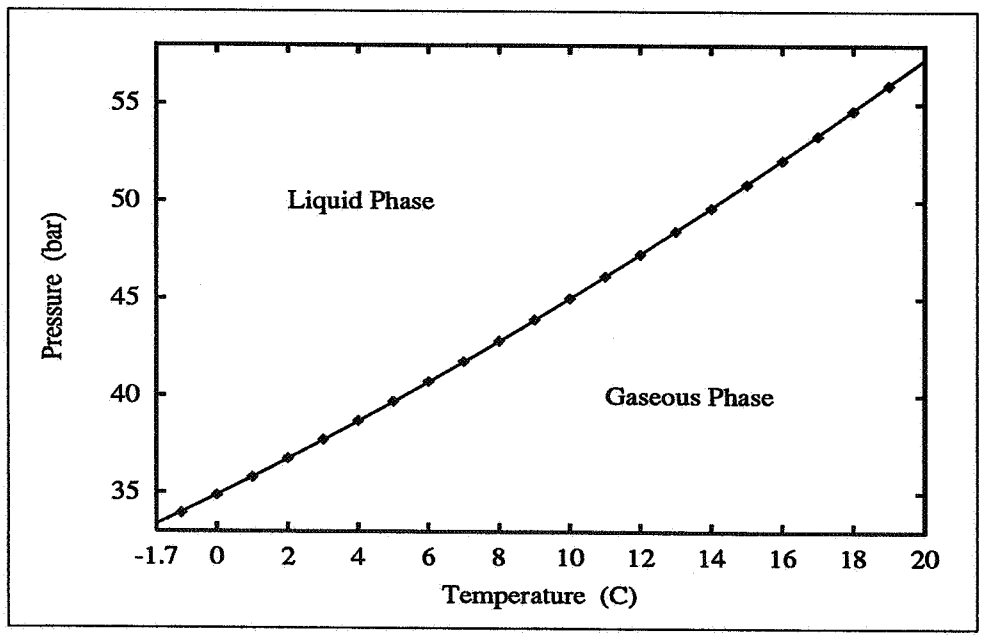

Figure 5: Condensation line for pure CO_2. The dots represent values from Weaset and Selby, 1967, the line represents a polynomial curve fit to the data points.

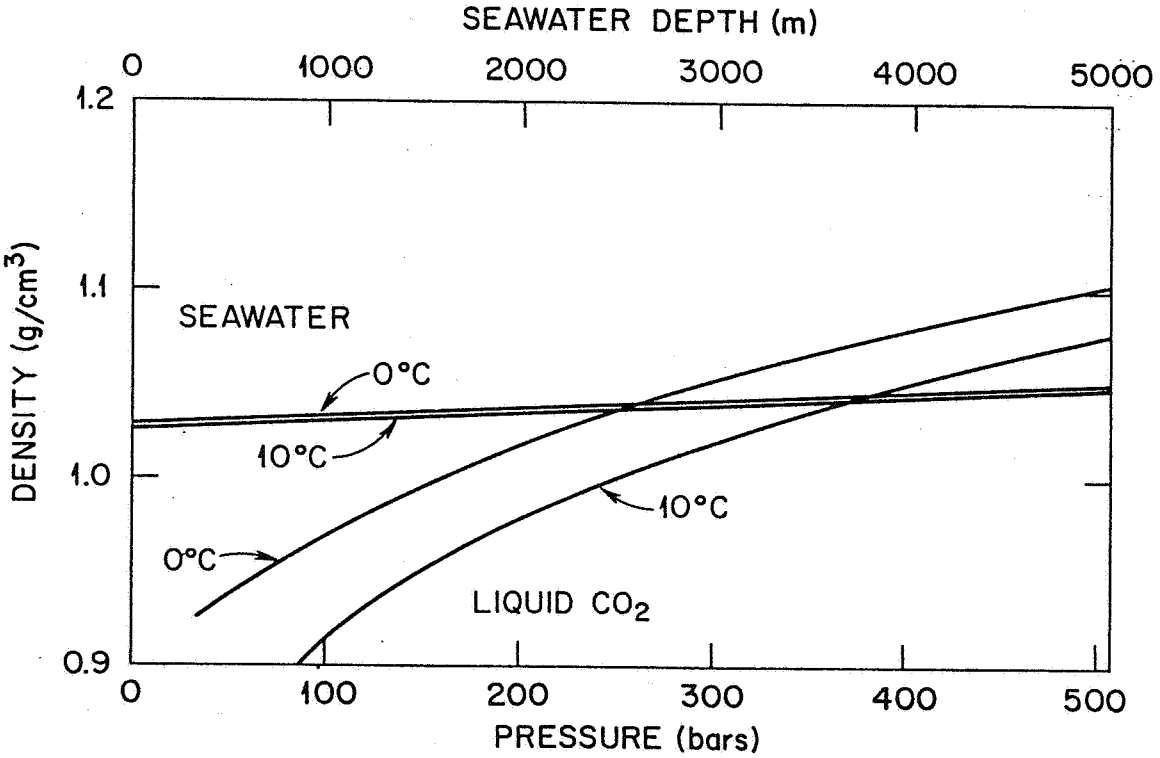

Figure 6: Density of liquid CO_2 and seawater at 0 and 10°C, and for pressures up to 500 bar. Figure from Baes *et al.*, 1980.

but heavier at larger depths. This means that liquid CO_2 has a positive bouyancy if released at depths shallower than about 3000 metres.

Many gases and easily volatile liquids in contact with water form a solid compound known as clathrate hydrate (King, 1969). For CO_2 in freshwater, the dissociation pressure at 0°C is 12.64 bar, the dissociation temperature at 1.01 bar is −24.0°C, and the critical hydrate temperature and pressure are 10.2°C and 45.09 bar, respectively (King, 1969; Miller, 1974). The dissociation pressure and temperature denote the boundaries in a pressure-temperature diagram where hydrate formation is possible.

Mitsubishi, 1990, has considered CO_2 hydrate formation in 'ordinary' seawater, see Tab. 1. Assuming the density of 'ordinary' seawater equals 1028 kg m^{-3} (see Subsec. 3.7),

Water depth Mitsubishi, 1990 (m)	Pressure Computed (bar)	Temperature Mitsubishi, 1990 (°C)
166	17.7	1.6
201	21.2	3.3
236	24.8	4.7
271	28.3	5.6
341	35.4	7.4
412	42.5	8.6
482	49.6	9.7
553	56.7	10.6

Table 1: Observed depth and temperature for CO_2 hydrate formation. The pressure is computed as the hydrostatic pressure assuming a seawater density of 1028 kg m^{-3}.

we have computed the hydrostatic pressures corresponding to the depths given in Tab. 1. A curve fit routine in the *Mathematica* package has been used to correlate the pressures and temperatures in Tab. 1. The CO_2 hydrate line in seawater, expressed by the hydrate pressure P_{hyd} (bar), is approximately given by the expression

$$P_{\mathrm{hyd}}(T_c) = 16.3639 + 0.336642 \cdot T_c + 0.308752 \cdot T_c^2 + 0.0000517535 \cdot \exp(T_c)\,, \qquad (13)$$

where T_c is temperature in degrees Celcius. P_{hyd} is plotted in Fig. 7. Since there are no datapoints for temperatures below 1.6°C, Eq. 13 should not be used for temperatures below 1°C.

Hydrate formation is only possible in the region above and to the left of the curves in Fig. 7. This means that hydrate formation cannot occur in waters warmer than about 10°C, at least not for oceanic pressures (Miller, 1974). The discontinuity point on the freshwater hydrate line at 10.2°C corresponds to the transition beween the gaseous and liquid CO_2 phases. According to King, 1969, the hydrate line rises very sharply with rise of temperature for pressures greater the condensation pressure. The reason for this is that the fugacity of a condensed phase varies only slowly with pressure at a given temperature. We address this point further in Subsec. 3.4.

The density of CO_2 hydrate is, according to Mitsubishi, 1129 kg m^{-3}, and the density is affected little by temperature and pressure. The density of seawater is less than 1050 kg m^3, which means that the CO_2 hydrate will sink to the bottom of the ocean.

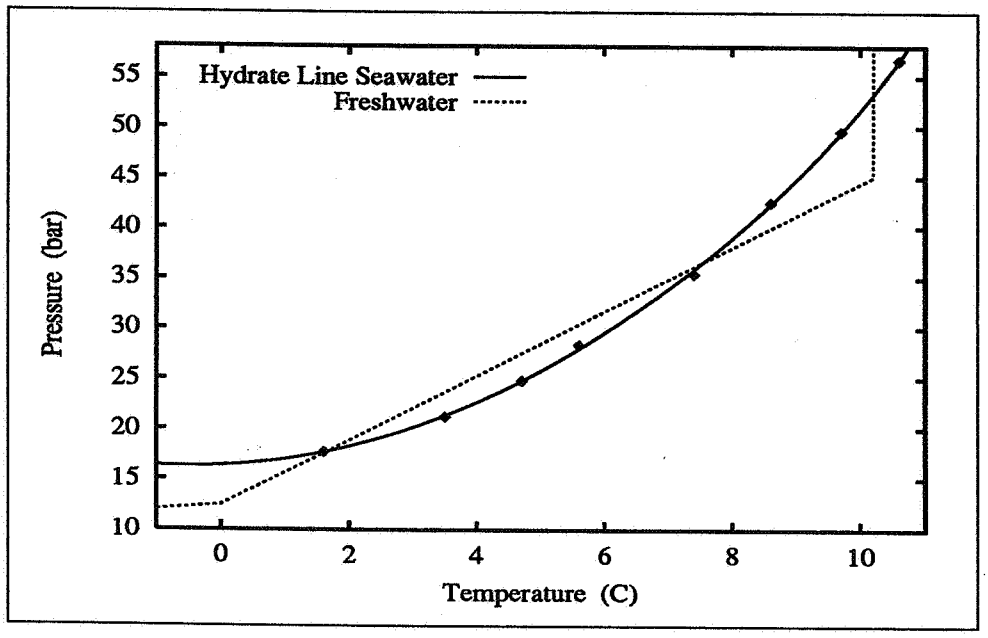

Figure 7: CO_2 hydrate lines for freshwater (after King, 1969) and seawater (data points after Mitsubishi, 1990). The hydrate line for seawater is given by Eq. 13.

Baes *et al.*, 1980, mention dry ice as a possible ocean disposal option. The density of dry ice is about 1500 kg m^{-3}, so blocks of dry ice will sink rapidly in the ocean. CO_2 hydrate or CO_2-enriched seawater are possible reaction products as the blocks sink through the water column. If the production and transport of dry ice can be justified from an energy and economic point of view, sinking blocks of dry ice will be efficient carriers of anthropogenic CO_2 to the deep ocean. We do not explicitly discuss the dry ice option in this paper. The theory to be developed is, however, directly applicable to the dry ice reaction products.

3.3 Equation of State for CO_2

The eigth-parameter Benedict-Webb-Rubin (BWR) equation of state is known to predict fairly accurately the thermodynamic properties of pure substances like carbon dioxide and methane, and complex hydrocarbon systems. The equation can be put in the form (Bishnoi and Robinson, 1971):

$$\frac{P\bar{V}}{RT} = 1 + \left(B_0 - \frac{A_0}{RT} - \frac{C_0}{RT^3}\right)\cdot\frac{1}{\bar{V}} + \left(b_0 - \frac{a_0}{RT}\right)\frac{1}{\bar{V}^2} + \frac{a_0\alpha}{RT}\cdot\frac{1}{\bar{V}^5}$$
$$+ \frac{c_0}{RT^3\bar{V}^2}\cdot\left(1 + \frac{\gamma}{\bar{V}^2}\right)\cdot\exp\left(-\frac{\gamma}{\bar{V}^2}\right). \qquad (14)$$

In Eq. 14, P (bar) is the pressure, $\bar{V}$ (L $mole^{-1}$) the molar volume of the gas, T (K) the absolute temperature, and the gas constant $R = 0.083144$ bar L K^{-1} $mole^{-1}$. The numerical values of the eight parameters in Eq. 14 are given in Tab. 2 for pure CO_2 (Bishnoi and Robinson, 1971; and Weiss, 1974).

A_0 L^2 bar $mole^{-2}$	B_0 L mole	C_0 L^2 K^2 bar $mole^{-2}$	a_0 L^3 bar $mole^{-3}$
1.9780606	0.033065171	172708.01	0.2559918

b_0 L^2 $mole^{-2}$	c_0 L^3 K^2 bar $mole^{-3}$	α L^3 $mole^{-3}$	γ L^2 $mole^{-2}$
6.6041298×10^{-3}	19851.606	4.7117009×10^{-5}	4.3414415×10^{-3}

Table 2: Values of the BWR parameter set for pure CO_2.

A much simpler equation of state is the two-parameter van der Waals equation

$$P = \frac{RT}{\bar{V} - b} - \frac{a}{\bar{V}^2}, \tag{15}$$

with the nomenclature of Eq. 14. Standard literature values for a and b for pure CO_2 are $a = 3.637$ L^2 bar $mole^{-2}$, and $b = 0.0427$ L $mole^{-1}$ (Laider and Meiser, 1982). We have found that a modification of these two parameters, namely

$$a = 4.1098 \text{ } L^2 \text{ bar } mole^{-2} \quad \text{and} \quad b = 0.03824 \text{ L } mole^{-1}, \tag{16}$$

leads to only small (max 2%) deviations between the BWR and the van der Waals equations for temperatures between 5 and 20°C.

The concentration C_{CO_2} of the CO_2-gas can be taken as the inverse of the molar volume;

$$C_{CO_2} = \bar{V}^{-1} = n/V, \tag{17}$$

where V is the volume and n the number of moles of the gas. In Fig. 8, the BWR equation and the van der Waals equation with standard literature and the modified parameter values for a and b are plotted as functions of P and C_{CO_2}. It is clear from this figure that the van der Waals equation with standard a- and b-values should not be used. Hereafter the 'modified van der Waals equation' means Eq. 15 with a and b given by (16).

3.4 Fugacity of CO_2

The fugacity f of a one-component nonideal gas is given by the expression (Levine, 1988)

$$\ln(f/P) = \int_0^P \left(\frac{\bar{V}}{RT} - \frac{1}{P} \right) dP, \tag{18}$$

for constant temperature T. In order to evaluate the integral in Eq. 18, we need a functional relationship between the pressure P and the molar volume $\bar{V}$. We have numerically solved the BWR-equation 14 with respect to $\bar{V}$ for a given P and T. The trapezoid rule has been used to approximate the integral in Eq. 18. The resulting fugacity is given in Tab. 3. The horizontal lines in the table indicate where CO_2 goes from the gaseous to the liquid phase;

Pressure (bar)	$T = 0°$ C	$T = 5°$ C	$T = 10°$ C	$T = 15°$ C	$T = 20°$ C
	Fugacity (bar)				
1.0	0.99	0.99	0.99	0.99	0.99
2.0	1.97	1.97	1.98	1.98	1.98
3.0	2.94	2.94	2.95	2.95	2.95
4.0	3.89	3.90	3.90	3.91	3.91
5.0	4.83	4.84	4.85	4.86	4.87
6.0	5.75	5.77	5.78	5.80	5.81
7.0	6.67	6.69	6.71	6.72	6.74
8.0	7.56	7.59	7.62	7.64	7.66
9.0	8.45	8.48	8.51	8.54	8.57
10.0	9.32	9.36	9.40	9.44	9.47
11.0	10.18	10.23	10.28	10.32	10.36
12.0	11.02	11.08	11.14	11.19	11.24
13.0	11.85	11.93	11.99	12.05	12.11
14.0	12.67	12.75	12.83	12.90	12.96
15.0	13.48	13.57	13.66	13.74	13.81
16.0	14.27	14.38	14.47	14.56	14.65
17.0	15.05	15.17	15.28	15.38	15.48
18.0	15.81	15.95	16.07	16.19	16.29
19.0	16.56	16.71	16.85	16.98	17.10
20.0	17.30	17.47	17.62	17.76	17.89
21.0	18.02	18.21	18.38	18.54	18.68
22.0	18.74	18.94	19.12	19.30	19.46
23.0	19.43	19.66	19.86	20.05	20.22
24.0	20.12	20.36	20.58	20.79	20.97
25.0	20.79	21.05	21.29	21.51	21.72
26.0	21.45	21.73	21.99	22.23	22.45
27.0	22.09	22.40	22.68	22.94	23.18
28.0	22.72	23.05	23.35	23.63	23.89
29.0	23.34	23.69	24.02	24.32	24.59
30.0	23.94	24.32	24.67	24.99	25.29
31.0	24.53	24.94	25.31	25.65	25.97
32.0	25.10	25.54	25.94	26.31	26.64
33.0	25.66	26.13	26.56	26.95	27.30
34.0	26.21	26.71	27.16	27.57	27.96
34.9	26.65	—	—	—	—
35.0		27.27	27.75	28.19	28.60
36.0		27.82	28.33	28.80	29.23
37.0		28.36	28.90	29.39	29.85
38.0		28.88	29.45	29.98	30.46
39.0		29.39	30.00	30.55	31.06
39.7		29.71	—	—	—
40.0			30.53	31.11	31.65
41.0			31.04	31.66	32.22
42.0			31.55	32.20	32.79
43.0			32.04	32.72	33.35
44.0			32.51	33.24	33.89
45.0			32.98	33.74	34.43
46.0				34.23	34.95
47.0				34.70	35.46
48.0				35.17	35.97
49.0				35.62	35.13
50.0				36.05	36.93
50.9				36.42	—
57.3					40.03
.					
70.9	28.88			38.15	

Table 3: The fugacity of carbon dioxide as function of temperature and pressure.

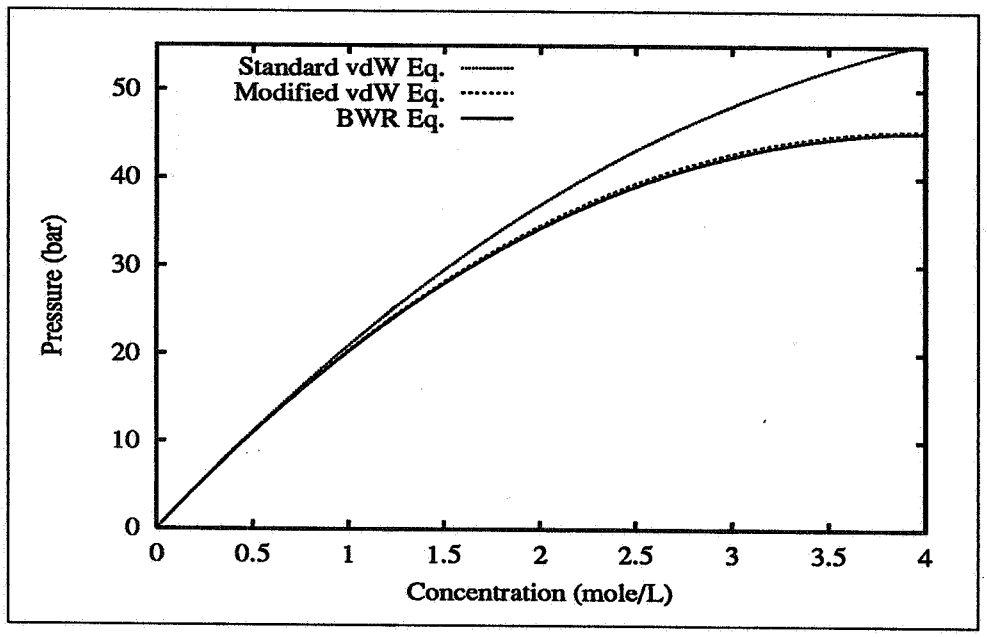

Figure 8: Three equations of state for CO_2: The standard and modified van der Waals equations, and the 'true' BWR equation. Temperature is set to 10°C.

the condensation pressures are taken from Eq. 12. The two numbers in the liquid domain are taken from King, 1969, and they indicate that the fugacity of a condensed phase varies only slowly with pressure at a given temperature. There is a nice agreement between the computed fugacity values in Tab. 3 and experimental/computed data given by King, 1969.

An approximate, explicit expression for the fugacity of CO_2 is

$$\ln(f/P) = \frac{b\,RT - a}{R^2T^2}\,P + \frac{2ab\,RT - a^2}{2\,R^4T^4}\,P^2\,. \tag{19}$$

This equation is based on a combination of the virial equation of state and the van der Waals equation, Eq. 15 (Levine, 1988). Once again we stress that the van der Waals parameters a and b should be taken from (16). Eq. 19, with a and b given by (16), approximates the 'true' fugacity fairly well for $P < 30$ bar.

3.5 Henry's Modified Law

The dissolution of carbon dioxide gas in water can be written as the 'reaction' (Stumm and Morgan, 1981)

$$CO_2(g) \rightleftharpoons CO_2(aq)\,, \tag{20}$$

where $CO_2(g)$ and $CO_2(aq)$ denote carbon dioxide in the gaseous and aquatic phases, respectively. At low pressures, the concentration of $CO_2(g)$, denoted $[CO_2(g)]$, can be expressed by Dalton's law of partial pressure:

$$[CO_2(g)] = pCO_2/RT\,. \tag{21}$$

Here pCO_2 (bar) denote the partial pressure of the CO_2 gas. 'Reaction' 20 can then be put in the form

$$[CO_2(aq)] = K_0\, pCO_2\,, \tag{22}$$

which is Henry's law. The constant K_0 is known as Henry's law constant, and has dimensions moles per (volume · pressure).

K_0 depends on temperature and salinity according to the equation (Weiss, 1974)

$$\begin{aligned}\ln K_0 = {} & A_1 + A_2\,(100/T) + A_3 \ln(T/100) \\ & + S \cdot \{B_1 + B_2(T/100) + B_3\,(T/100)^2\}\,,\end{aligned} \tag{23}$$

where T is absolute temperature in Kelvin, salinity S in pro mil, and K_0 in moles L^{-1} atm^{-1}. The A- and B-constants in Eq. 23 are given in Tab. 4. K_0 can easily be converted

A_1	A_2	A_3	B_1	B_2	B_3
−58.0931	90.5069	22.2940	0.027766	−0.025888	0.0050578

Table 4: The numerical values of the constants in Eq. 23 for K_0 is in moles L^{-1} atm^{-1}.

to moles L^{-1} bar^{-1} through the relation

$$1 \text{ atm} = 1.013250 \text{ bar}\,. \tag{24}$$

In Fig. 9, we have plotted the Henry's law constant for freshwater and two salinity extrema of seawater. As we see, freshwater can absorb more CO_2 than seawater. This result has important implications for the CO_2-sequestration problem: Use of the properties of freshwater results in too high estimates of the CO_2-absorption capacity of seawater. Furthermore, the Henry's law constant — and thereby the uptake capacity — of CO_2 in water/seawater increases with decreasing water temperature.

Henry's law in the form of Eq. 22 breaks down at pressures somewhat above atmospheric pressures. The equation

$$[CO_2(aq)] = K_0\, f_{CO_2} \exp[(1 - P)\bar{v}_{CO_2}/RT]\,, \tag{25}$$

known as the 'modified Henry's law equation', is used to represent the solubility of CO_2(g) in liquids at elevated pressures (King, 1969; Weiss, 1974). In Eq. 25, f_{CO_2} is the fugacity of carbon dioxide (Subsec. 3.4), and $\bar{v}_{CO_2}$ is the partial molar volume of CO_2(aq) in solution (see below). Henry's modified law is valid for CO_2 in freshwater and seawater for temperatures up to 40°C and over the pressure range 0–500 bar (King, 1969; and Weiss, 1974).

Since the numerical value of the exponential factor in Eq. 25 is close to one for $P < 30$ bar, we have that the solubility of CO_2 increases almost linearly with the fugacity f_{CO_2} for moderate pressures. For pressures higher than the condensation pressure, the fugacity increases very slowly with pressure, whereas the exponential factor decreases slowly. The solubility in the liquid phase, at least for the range of pressures we consider ($P \lesssim 50$ bar), may therefore be approximated by the solubility at the condensation pressure.

The results of this and the previous subsection are summarized in Fig. 10: For a given temperature, the solubility of CO_2 gas in water/seawater reaches its maximum at the condensation line. The solubility increases with decreasing temperature, so max solubility is obtained

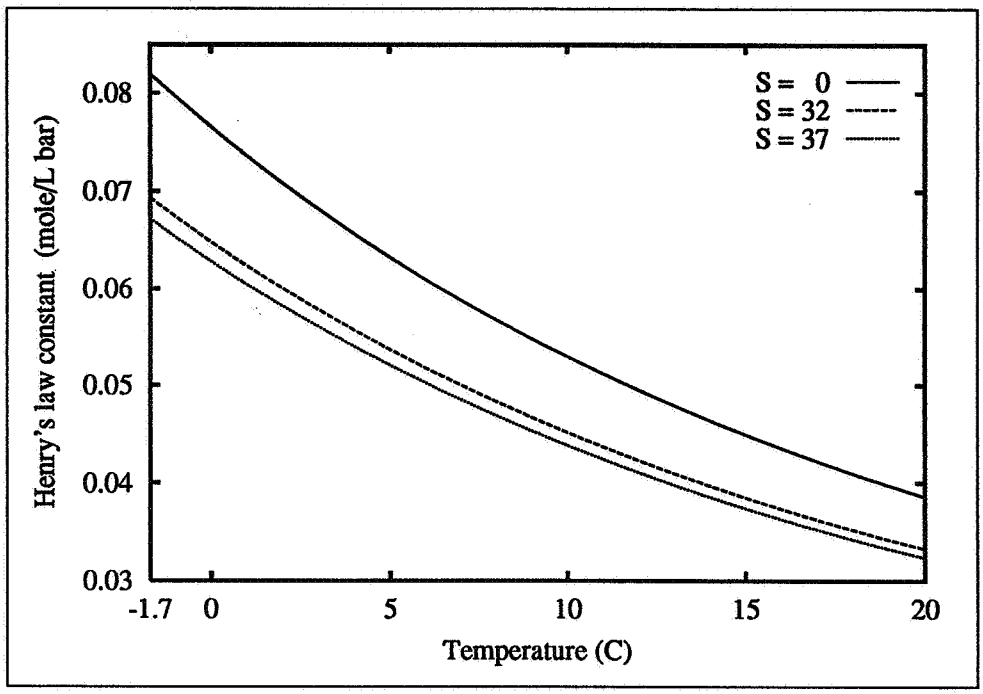

Figure 9: Henry's law constant for freshwater, and for seawater with salinity $S = 32$ and 37 pro mil. $-1.7°C$ indicates the freezing point for seawater at 35 pro mil salinity.

	$T = -1.7°C$	$T = 0°C$	$T = 5°C$	$T = 10°C$	$T = 15°C$	$T = 20°C$
	Dissolved CO_2 (moles m^{-3})					
Freshwater	—	1940	1770	1640	1520	1430
Seawater	1670	1620	1480	1380	1290	1210

Table 5: Dissolved CO_2 at the condensation pressure given by Eq. 12.

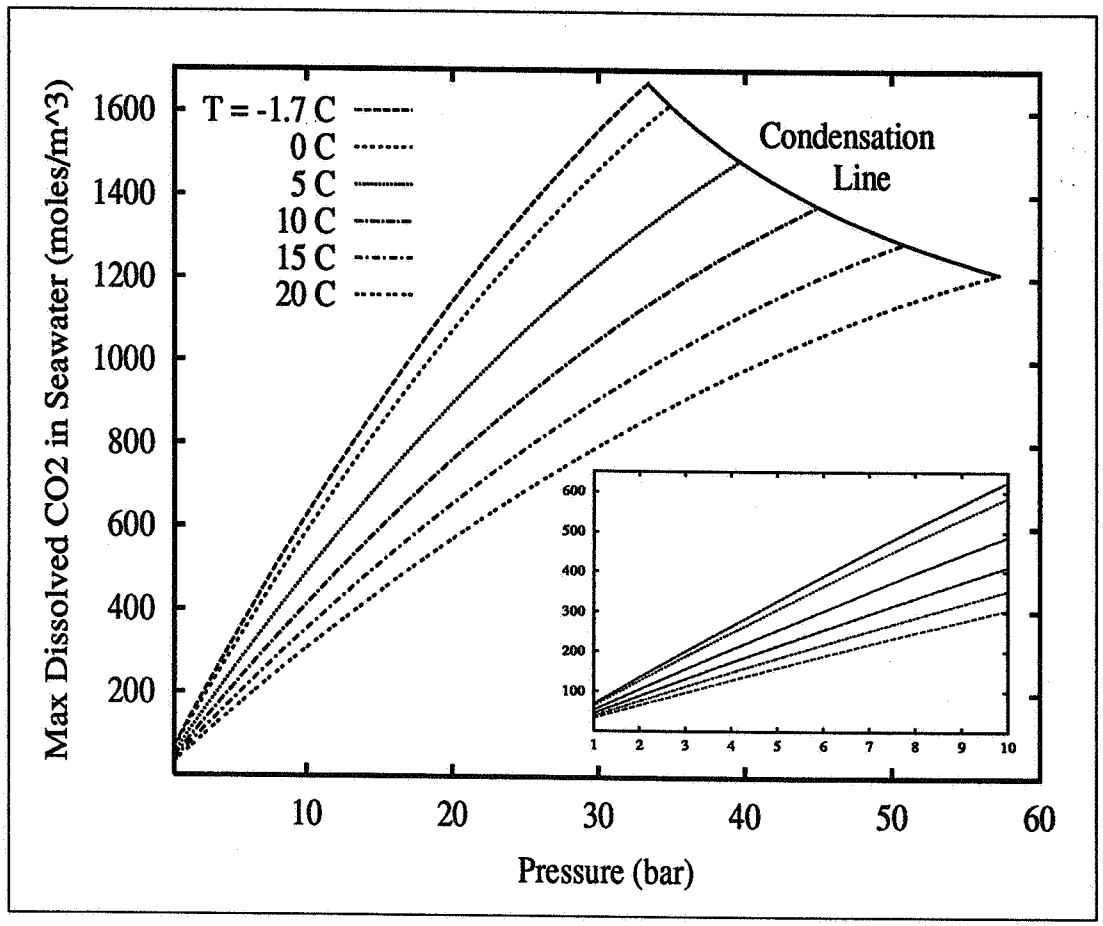

Figure 10: The CO_2 uptake capacity of seawater at 35 pro mil salinity computed from Eq. 25. The small figure shows the uptake capacity at low pressures. Labels as for the main figure.

at the freezing temperatures of the fluids (i.e. at 0°C for pure water and about −1.7°C for seawater at 35 pro mil salinity). Furthermore, the solubility increases with decreasing salinity (see Fig. 9).

Approximate numerical values of max dissolved CO_2 in freshwater and seawater ($S = 35$ pro mil) are given in Tab. 5. Notice that one m^3 seawater can absorb more than 1000 moles CO_2.

3.6 Partial Molar Volume of CO_2 in Water and Seawater

The partial molar volume of component i in solution is defined as (King, 1969)

$$\bar{v}_i = \left.\frac{\partial V'}{\partial n_i}\right|_{T,P,n_j} \tag{26}$$

where V' is the total volume of solution, and the subscripts T, P and n_j denote that the temperature, pressure and the components $j \neq i$ are held constant during the differentiation. Therefore, the quantity $\bar{v}_{CO_2}$ in Eq. 25 is a measure of the volume expansion of solution as CO_2(aq) is added to the solution.

It is possible to show that the variation of the volume $\bar{v}_i$ is negligibly small over the range of conditions in which Eq. 25 is valid (King, 1969). The constancy of $\bar{v}_i$ is also verified through measurements. For CO_2 in water, Kritchevsky and Iliinskaya, 1945, gave the values $\bar{v}_{CO_2} = 32$ cm^3 mole^{-1} for $T = 0$°C, 33 cm^3 mole^{-1} for $T = 25$, and 34 cm^3 mole^{-1} for 50°C. Weiss, 1974, found that $\bar{v}_{CO_2} = 32.3 \pm 0.5$ cm^3 mole^{-1} for CO_2 in pure water for temperatures between 12 and 40°C and for pressures up to 500 bar. In seawater with salinity 35 pro mil and temperature 23°C, Bradshaw, 1973, found that $\bar{v}_{CO_2} = 33.4 \pm 0.5$ cm^3 mole^{-1} for atmospheric pressures. Watanabe and Iizuka, 1985, give the following expression for $\bar{v}_{CO_2}$ in water at atmospheric pressure

$$\bar{v}_{CO_2} = 33.520 + 0.0071\, T_c, \tag{27}$$

where T_c is temperature in degrees Celcius. The above expression is derived from measurements for temperatures between 0 and 20°C. In Eq. 25 and in the following computations, we have used the conservative value $\bar{v}_{CO_2} = 34.0$ cm^3 mole^{-1}.

3.7 Density of Seawater

The density of seawater is given by the socalled UNESCO-formula (UNESCO, 1981). Fig. 11 shows seawater density at 35 pro mil salinity as a function of pressure and temperature. From this figure we see that a typical density of seawater for temperatures between 5–10°C and at 35 pro mil salinity is about 1028 kg m^{-3}. An upper limit for the density of seawater in the upper 500 metres of the ocean can be taken as 1030 kg m^{-3}.

3.8 Heat of Solution

When CO_2(g) dissolves in water, heat is released. The heat of solution H can be calculated from solubility data of CO_2 in water, and King, 1969, gives the value

$$H = 5.9 \text{ kcal mole}^{-1} \approx 2.5 \times 10^4 \text{ J mole}^{-1}. \tag{28}$$

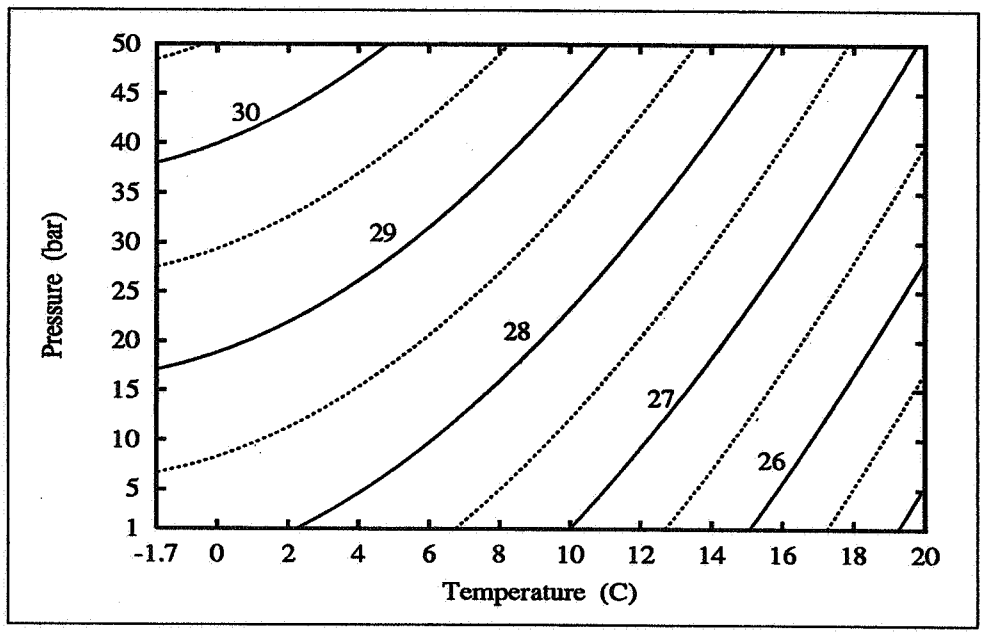

Figure 11: Density of seawater at 35 pro mil salinity. The numbers correspond to the solid lines, and give the density in terms of $(\rho_w - 1000)$ kg m^{-3}. The dotted lines are 0.5 kg m^{-3} contours.

This value is assumed to be a conservative (high) value of the heat of solution for pressures up to the condensation pressure.

The heat capacity c_p of seawater at 35 pro mil salinity, for $T_c < 20°C$ and $P < 100$ bar, is about 4.0 J kg^{-1} K^{-1} (Millero *et al.*, 1973). A conservative (low) value of the seawater density for depths less than 500 metres can be taken as 1020 kg m^{-3} (Subsec. 3.7). We then have that

$$c_p \approx 4.1 \times 10^6 \text{ J m}^{-3} \text{ K}^{-1}. \tag{29}$$

The temperature increase of seawater due to released heat of solution is given by

$$H/c_p \approx 6.1 \times 10^{-3} \text{ K m}^3 \text{ mole}^{-1}. \tag{30}$$

This means that one mole CO_2 dissolved in one m^{-3} of seawater leads to a temperature increase of about 6×10^{-3} K.

3.9 Density of CO_2-Enriched Seawater

From the previous subsections we know that the concentration of inorganic carbon dioxide C_T in seawater can be artificially increased from the natural level of about 2.2 to above 1000 moles m^{-3}. Any increase in C_T is accompanied by a change in seawater volume. From Subsec. 3.1, we have that variations in the C_T-concentration above 3.5 moles m^{-3} are well approximated by variations in $CO_2 + H_2CO_3$. The volume expansion of seawater is then given by $\bar{v}_{CO_2}$ (Watanabe and Iizuka, 1985).

Let $\rho_w^0 = m_w^0/V_w^0$ denote the density of natural, or ambient, seawater. m_w^0 and V_w^0 are the corresponding mass and volume of seawater. The mass of artificially added CO_2, m_{CO_2}, is given by the expression

$$m_{CO_2} = n_{CO_2} \cdot M_{CO_2}, \tag{31}$$

where n_{CO_2} is the number of moles of CO_2 added to the seawater and $M_{CO_2} = 44.01 \times 10^{-3}$ kg mole^{-1} is the molar mass of CO_2. The addition of n_{CO_2} moles CO_2 leads to a volume expansion V_{CO_2} given by the expression

$$V_{CO_2} = n_{CO_2} \cdot \bar{v}_{CO_2}. \tag{32}$$

Experimental values for $\bar{v}_{CO_2}$ in freshwater and seawater are given in Subsec. 3.6. The change in seawater density $\Delta\rho_w$ is given by the difference between the density of the CO_2-enriched and the ambient seawater:

$$\begin{aligned}\Delta\rho_w &= \frac{m_w^0 + m_{CO_2}}{V_w^0 + V_{CO_2}} - \frac{m_w^0}{V_w^0} \\ &= n_{CO_2} \frac{M_{CO_2} V_w^0 - m_w^0 \bar{v}_{CO_2}}{V_w^0 (V_w^0 + n_{CO_2} \bar{v}_{CO_2})} \\ &= (M_{CO_2} - \rho_w^0 \bar{v}_{CO_2}) \cdot \Delta C_T. \end{aligned} \tag{33}$$

In Eq. 33,

$$\Delta C_T \overset{\text{def}}{=} \frac{n_{CO_2}}{V_w^0 + n_{CO_2} \bar{v}_{CO_2}} \tag{34}$$

denote the change in the total carbon concentration C_T due to the added CO_2.

So far we have neglected the effect from the heat of solution on ρ_w. Since $\rho_w = \rho_w(C_T, T)$, we have that the change in seawater density due dissolution of CO_2(g), or increase in C_T, is given by the expression

$$\frac{d\rho_w}{dC_T} = \frac{\partial\rho_w}{\partial C_T} + \frac{\partial T}{\partial C_T} \frac{\partial\rho_w}{\partial T}. \tag{35}$$

The first term on the right hand side of expression (35) is given by Eq. 33:

$$\frac{\partial\rho_w}{\partial C_T} = M_{CO_2} - \rho_w^0 \bar{v}_{CO_2}. \tag{36}$$

The $\partial T/\partial C_T$-factor is given by Eq. 30, so Eq. 35 becomes

$$\frac{d\rho_w}{dC_T} = (M_{CO_2} - \rho_w^0 \bar{v}_{CO_2}) + \frac{H}{c_p} \frac{\partial\rho_w}{\partial T}, \tag{37}$$

where $H/c_p \approx 6.1 \times 10^{-3}$ K m^3 mole^{-1}.

From Fig. 11, we see that the thermal expansion factor $\partial\rho_w/\partial T$ is negative, and that $|\partial\rho_w/\partial T|$ increases with temperature. Some values of $|\partial\rho_w/\partial T|$ for seawater at 35 pro mil salinity are given in Tab. 6.

Eq. 37 is illustrated in Fig. 12. In part (a) of the figure, we have plotted the right hand side of Eq. 37 as function of temperature and pressure. We see that the first term of the right hand side varies very little with temperature, whereas the thermal expansion effect becomes appreciable at high temperatures. Part (b) shows the maximum increase in seawater density for a given temperature and pressure. As we see, a density increase of more than 10 kg m^{-3} is possible. Notice that the curves in Fig. 12(b) show the density effect associated with the maximum CO_2 uptake capacity of seawater given by Fig. 10.

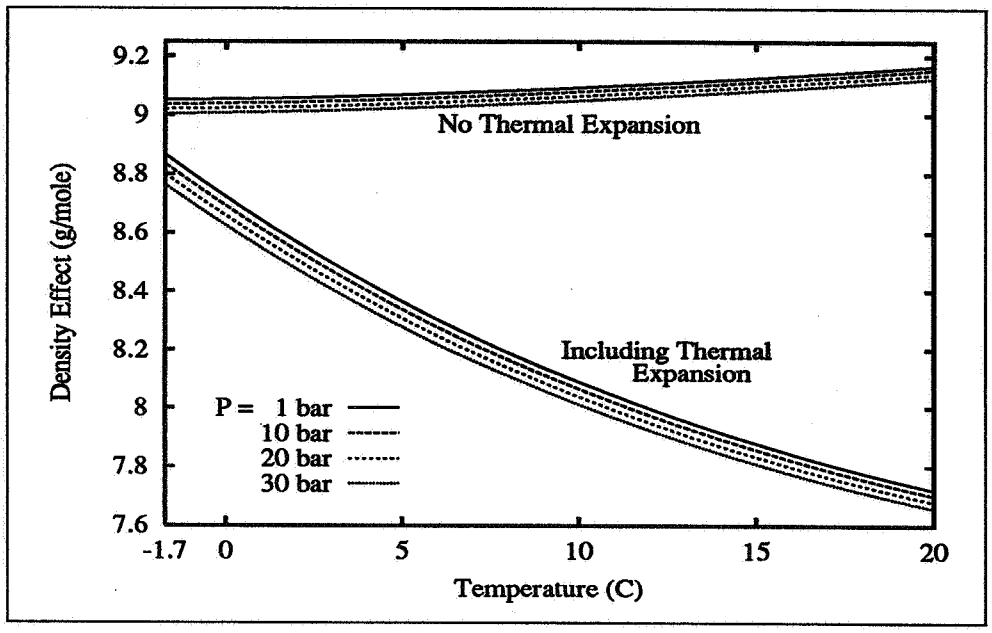

(a) The right hand side of Eq. 37 with and without the thermal expansion term.

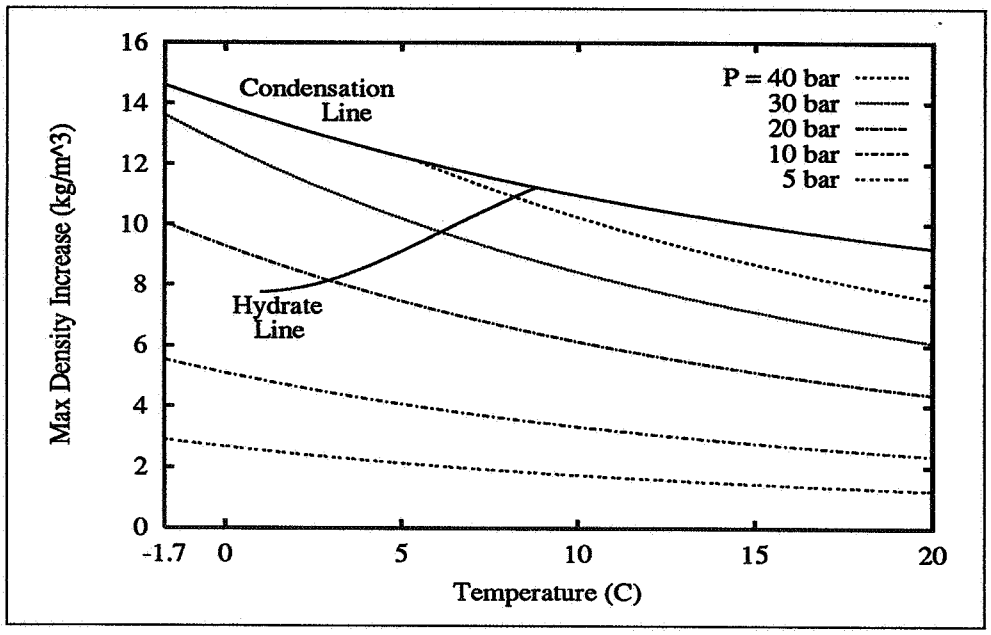

(b) Maximum increase in density of CO_2-enriched seawater as function of temperature and pressure. Computed from Eq. 37, and where the change in C_T concentration is computed by Henry's modified law (Eq. 22). The hydrate line is given by Eq. 13, and CO_2 hydrate formation is only possible above the hydrate line.

Figure 12: The changes in seawater density connected with artificial addition of CO_2. $S = 35$ pro mil, $\bar{v}_{CO_2} = 34$ cm^3 mole^{-1}, $H = 2.5 \times 10^4$ J mole^{-1}, $\partial\rho_w/\partial T$ is computed from the the equation of state of seawater (UNESCO, 1981), and c_p from Millero *et al.*, 1973.

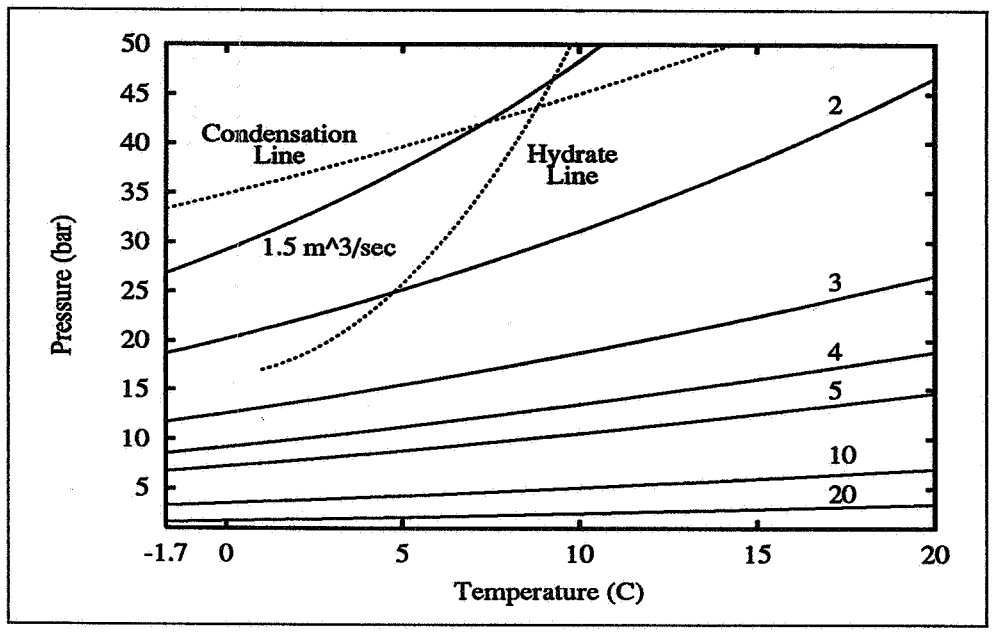

(a) The contours are expressed in $m^3\ s^{-1}$. The hydrate line is given by 13, and the condensation line by Eq. 12.

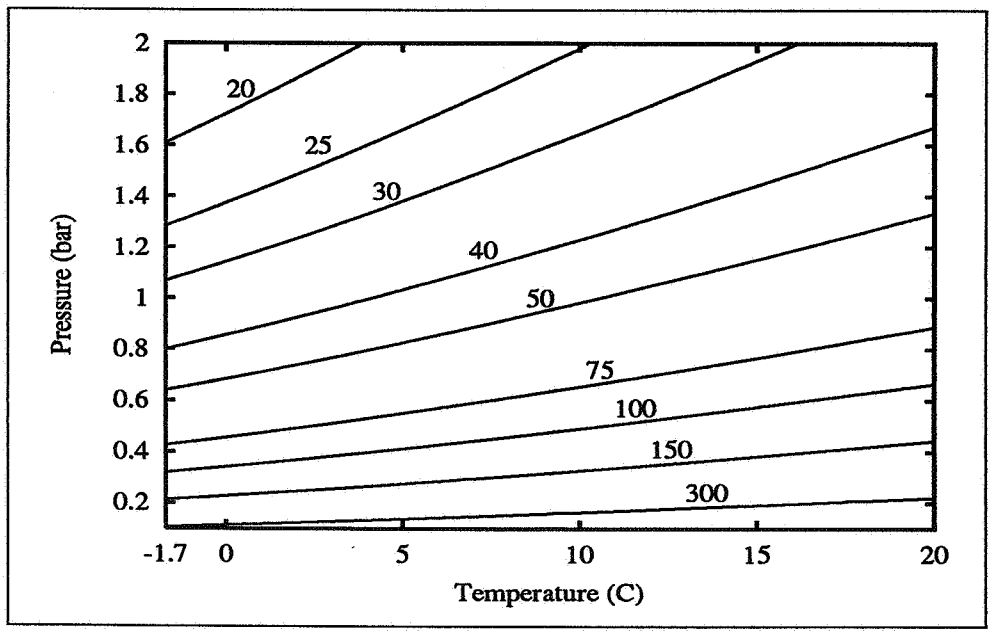

(b) The contours are expressed in $m^3\ s^{-1}$.

Figure 13: Flux of seawater needed in order to absorb the CO_2 produced by a 1 GW gas power plant. The contours are computed from Eq. 38, and the dimensions of the flux numbers are $m^3\ s^{-1}$. Salinity is set to 35 pro mil.

Pressure (bar)	Temperature (°C)						
	-2	0	4	10	13	16	19
0	0.0261	0.0541	0.1049	0.1713	0.2010	0.2287	0.2551
100	0.0570	0.0825	0.1292	0.1902	0.2176	0.2434	0.2679

Table 6: $|\partial\rho_w/\partial T|$ for seawater at 35 pro mil salinity. Values computed from Gill, 1982.

3.10 Minimum Seawater Flux for Dissolution of the Emissions From a 1 GW Gas Power Plant

Based on the maximum CO_2 uptake capacity of seawater, we have computed the seawater renewal rate needed in order to absorb 3×10^9 kg CO_2 per year; the estimated emissions from a 1 GW gas power plant (Norwegian State Pollution Authority, personal comm.). The needed seawater flux F is given by the expression

$$F = \frac{2.2 \times 10^3}{[CO_2(aq)]} \text{ m}^3 \text{ s}^{-1}, \tag{38}$$

where the numerator represents the emissions in moles per second, and $[CO_2(aq)]$ (moles m^{-3}) is given by Eq. 25. Some values of F are plotted in Fig. 13 as functions of temperature and pressure. As we see, a rather low water flux is needed in order to absorb the 2.2×10^3 moles CO_2 produced per second.

A conservative (low) estimate of the oceanic current velocities off the Norwegian coast is 0.1 m s^{-1}. If the produced CO_2 is injected into the ocean at depths greater than about 150 metres, the injected CO_2 has to be spread over a cross-stream area of 30 m^2 in order to be absorbed.

It is important to notice that expression (38) gives the minimum seawater flux needed in order to absorb the CO_2 released from the gas power plant. Depending on the efficiency of the CO_2-seawater dissolution device, the real seawater flux is expected to lie between F and $2F$.

3.11 Summary

The main results of this section are shown in Figs. 10, 12(b) and 13, and they are reproduced in Tab. 7. The CO_2 uptake capacity of seawater increases with increasing pressure and decreasing temperature. At pressure of 20 bar and temperature of 5°C, about 900 moles CO_2 may be dissolved per m^3 water. The density increase of the CO_2-enriched seawater is then about 7.4 kg m^{-3}. Even a fraction of this density increase will lead to sinking plumes of CO_2-enriched seawater. The temperature of the intermediate water off the Norwegian coast is typically between 4 and 8°C. These waters are therefore able to absorb substantial amounts of CO_2 without hydrate formation.

We also see that there is a dramatic difference in the seawater flux needed to absorb the CO_2 produced by a 1 GW gas power plant for low (i.e. $pCO_2 \lesssim 0.5$ bar) and high (i.e. $pCO_2 \gtrsim 5$ bar) pressures.

Pressure (bar)	Temperature (°C)			
	0	5	10	15
0.2	13	11	9	8
0.5	31	26	22	19
1	63	53	44	38
5	310	250	210	180
10	590	490	410	350
20	1070	900	760	660
30	1460	1230	1050	910
P_{cond}	1620	1480	1380	1290

(a) Max CO_2 (moles m^{-3}) dissolved in seawater. Computed from Eq. 25.

Pressure (bar)	Temperature (°C)			
	0	5	10	15
0.2	0.1	0.09	0.07	0.06
0.5	0.3	0.2	0.2	0.1
1	0.6	0.4	0.4	0.3
5	2.7	2.1	1.7	1.4
10	4.9	4.1	3.3	2.8
20	8.9	7.4	6.1	5.2
30	13	10	8	7
P_{cond}	14	12	11	10

(b) Density increase (kg m^{-3}) of CO_2-enriched seawater. Computed from Eq. 37.

Pressure (bar)	Temperature (°C)			
	0	5	10	15
0.2	170	205	244	286
0.5	68	82	98	115
1	34	41	49	58
5	7	9	10	12
10	4	4	5	6
20	2	2	3	3
30	1.5	1.8	2.1	2.4
P_{cond}	1.3	1.4	1.6	1.7

(c) Minimum seawater flux (m^3 s^{-1}) needed in order to absorb the amount of CO_2 released from a 1 GW gas power plant. Computed from Eq. 38.

Table 7: The main results of this section. Salinity is set to 35 pro mil in all of the computations. P_{cond} denotes the condensation pressure, and is given by Eq. 12.

4 Bubble Dynamics

In this section the stability and velocity of ascending gas-bubbles in water are studied. A numerical bubble model is developed, and this model is used to determine the dissolution rates of ascending CO_2 bubbles in seawater.

4.1 Spherical, Ellipsoidal and Cap Particles

Bubbles and drops in free rise or fall in infinite media can generally be put in one of the following three categories (Clift *et al.*, 1978): Spherical, ellipsoidal and cap-shaped particles. Numerical values of two of the following dimensionless numbers,

$$\text{Eötvös number:} \quad \text{Eo} = \frac{4g|\rho_p - \rho_w|r^2}{\sigma},$$

$$\text{Morton number :} \quad \text{M} = \frac{g\mu_w^4|\rho_p - \rho_w|}{\rho_w^2\sigma^3},$$

$$\text{Reynolds number:} \quad \text{Re} = \frac{2\rho_w r U_T}{\mu_w},$$

can be used to identify the actual shape regime for bubbles and drops in fluids, as shown in Fig. 14. In the following, the continuous and dispersed fluids are identified by the subscripts w (for water/seawater) and p (for particle), respectively. Here particle means either bubbles or drops. In the above expressions, $g = 9.8$ m s^{-1} is the gravitational acceleration; ρ (kg m^{-3}) is the density; r (m) is the equivalent radius of the particle; σ (kg s^{-2}) the surface or interfacial tension; μ (kg m^{-1} s^{-1}) the viscosity; and finally U_T (m s^{-1}) the terminal velocity of the particle.

The equivalent radius of a non-spherical particle with volume V is taken as the radius r of the volume-equivalent sphere, so

$$r = \left(\frac{3}{4\pi}V\right)^{1/3}.$$

The surface tension σ of clean water is given by the expression (Riley and Skirrow, 1975)

$$\sigma = (75.64 - 0.144 \cdot T_c + 0.0221 \cdot S) \times 10^{-3} \text{ kg s}^{-2}, \tag{39}$$

where T_c is temperature in degrees Celcius and S salinity in pro mil.

Tab. 8 gives the viscosity of freshwater and some common seawater salinities as functions of temperature.

Fig. 14 applies for a very broad group of bubbles and drops in fluids, the most important exception is for liquid drops falling through gases. Furthermore, the viscosity of the fluid particle μ_p (not included in the definitions of Eo, M and Re) should be taken into account for very pure (i.e. surfactant-free) systems, and for large particles in high M liquids. In general, gas bubbles in water with $r \lesssim 9$ mm are in the ellipsoidal regime, whereas bubbles with $r \gtrsim 9$ mm are in the cap-shaped regime.

4.2 Break-Up of Rising Bubbles in Stagnant Liquids

Grace *et al.*, 1978, have considered both experimental and theoretical models for break-up of bubbles in stagnant media. The theoretical analysis is based on the growth of waves on

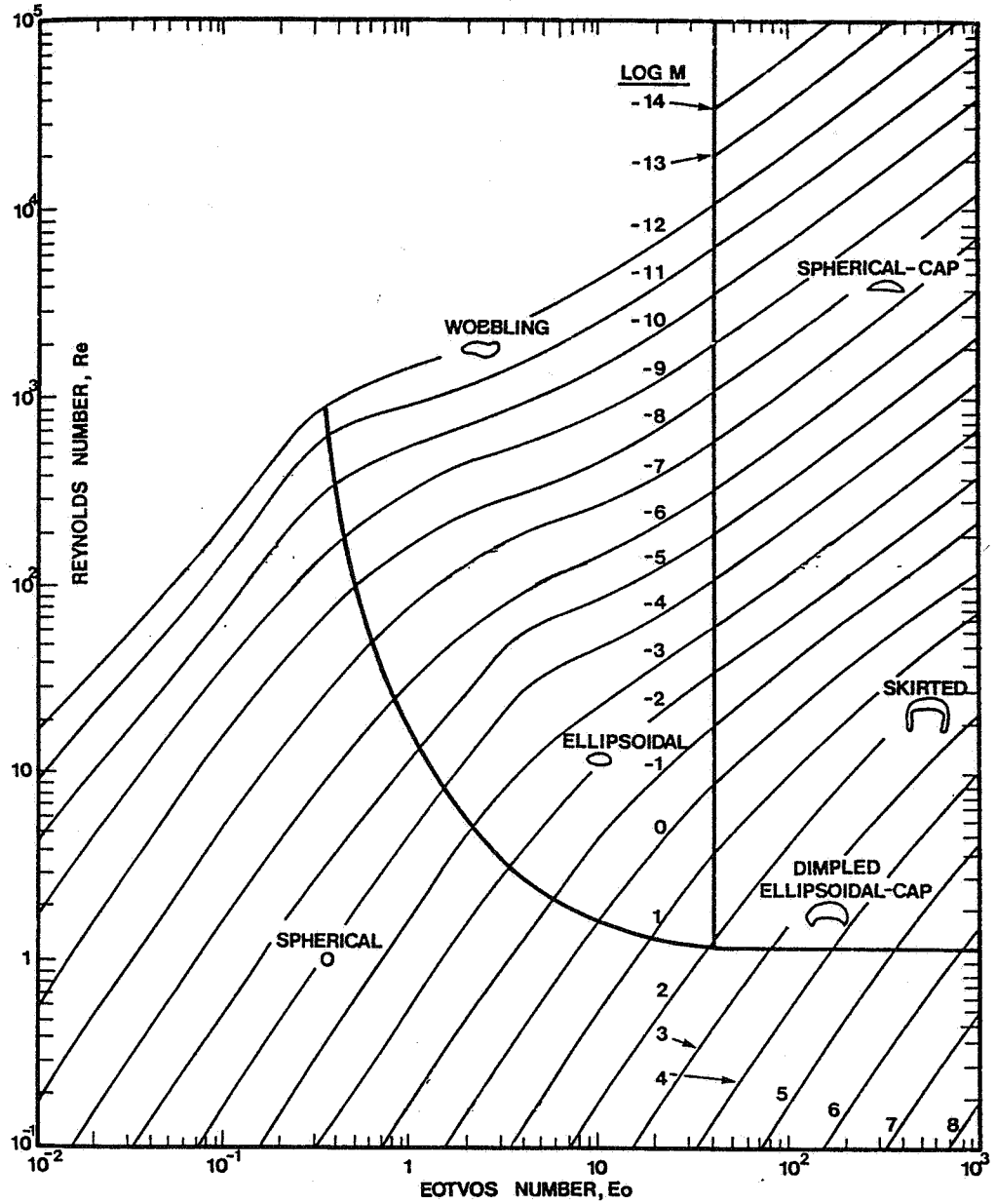

Figure 14: Shape regimes for free falling or ascending bubbles and drops in fluids. Figure after Clift *et al.*, 1978.

Salinity (pro mil)	Temperature (°C)					
	0	4	8	12	16	20
0	1.7916×10^{-3}	1.5681×10^{-3}	1.3857×10^{-3}	1.2349×10^{-3}	1.1087×10^{-3}	1.0020×10^{-3}
32	1.8767	1.6427	1.4607	1.3057	1.1758	1.0658
34	1.8823	1.6528	1.4652	1.3101	1.1800	1.0698
36	1.8876	1.6578	1.4701	1.3146	1.1841	1.0737

Table 8: The viscosity μ_w (kg m^{-1} s−1) of freshwater and seawater. Data from Riley and Skirrow, 1975.

a density discontinuity, i.e. a Rayleigh-Taylor instability analysis. They have not explicitly looked at break-up of bubbles in water, but they predict a maximum stable bubble radius of about 2.5 cm for this case. We have two comments to the work by Grace *et al.* First of all, the Rayleigh-Taylor instability does not include the relative motion of the dispersed and continuous fluids. This means that generation of instability due to velocity shear is not included. Secondly, disturbances are assumed to propagate along the bubble-water interface by Stokes flow, while potential flow would be more appropriate.

Kitscha and Kocamustafaogullari, 1989, have considered both the Rayleigh-Taylor and Kelvin-Helmholtz instabilities in the break-up process. The Kelvin-Helmholtz theory allows relative motion between the dispersed and the continuous fluids. The theoretical break-up radius for air-bubbles in water is found to be about 4 cm. However, it is difficult to check the validity of this critical radius value because of the small number of available data.

We also have a comment to the work by Kitscha and Kocamustafaogullari. They seem to pick out the least instable mode as the leading mode in the break-up process. This assumption might be consistent with the linear theory, but we expect that other and more unstable modes will lead to splitting. This should imply that the given theoretical break-up radius represents a conservative upper limit for the maximum size of gas-bubbles in water.

In addition to the above mentioned stability analysis, Batchelor, 1987, discusses the effect of the deforming motion of the liquid adjoining the bubble interface. Again it is difficult to test the theoretical model due to the lack of observations of the maximum size of gas bubbles in water.

Wilkinson and v. Dierendonck, 1990, have studied the effect of pressure and gas density on the bubble size. They found that the bubble size decreased quite dramatically with increased pressure and gas density. If similar effect can be found to apply to our bubble syste, it would mean rapid break-up of the large bubbles when injection takes place at depths of 100 metres or more.

All in all, there is a serious need for experimental values of the maximum stable bubble radius for gas-bubbles in water. In lack of something better, we have taken 3 cm as the maximum bubble radius. This radius might be too small for bubbles in the uppermost 50–100 metres of the ocean, but is expected to describe bubble break-up from about 100 metres and down to the condensation depth of CO_2.

Before we close this subsection, let us mention that bubbles may have radii larger than the critical radius for several seconds before the instability is strong enough to split the bubble. This means that break-up experiments should be carried out in at least 15–20 metres high bubble columns. Furthermore, bubbles tend to break-up more easily in turbulent than stagnant water. Break-up of a single bubble in stagnant water therefore overestimates the break-up radius for an ensemble of bubbles in water.

4.3 Terminal Velocities for Gas Bubbles in Water

A particle in a stagnant fluid experiences forces due to gravity and buoyancy, in addition to resisting drag forces. The net gravitational force F_G acting on a spherical particle of radius r and density ρ_p is

$$F_G = \frac{4}{3}\pi r^3 g(\rho_p - \rho_w)\,. \tag{40}$$

When the gravitational and drag forces balance, the particle describes a constant settling or ascending velocity; the terminal velocity. The terminal velocity generally depends on

hydrodynamic properties of the fluid and the radius and density of the particle.

For bubbles in pure water with $r > 0.7$ mm, the terminal velocity can be expressed as (Clift *et al.*, 1978, with the factor 0.98 set to unity)

$$U_T = 0.98\sqrt{(1.07\,\sigma/r\rho_w) + 1.01\,gr}\,. \tag{41}$$

The terminal velocity for bubbles with $r \lesssim 1$ cm in contaminated water is slightly less than U_T given by Eq. 41 (Clift *et al.*). The effect of non-negligible gas density is included in the expression (Clift *et al.*, 1978)

$$U_T = \sqrt{rg\,\frac{\rho_w - \rho_p}{\rho_w}}\,. \tag{42}$$

Eq. 42 is valid for bubbles satisfying the following conditions: M $< 10^{-2}$, Eo ≥ 40 and Re $\gtrsim 150$, and these conditions are generally satisfied for air bubbles in water for bubble-radii $r \gtrsim 9$ mm.

The density ρ_{CO_2} of the CO_2-gas as a function of pressure can be taken from Fig. 8, since $\rho_{CO_2} = C_{CO_2} \cdot M_{CO_2}$ ($M_{CO_2} = 44.01 \times 10^{-3}$ kg mole^{-1}). For $P = 10$ bar, $\rho_{CO_2} \approx 20$ kg m^{-3}, and for $P = 30$ bar, $\rho_{CO_2} \approx 70$ kg m^{-3}. These density estimates hold for temperatures between 0 and 20°C.

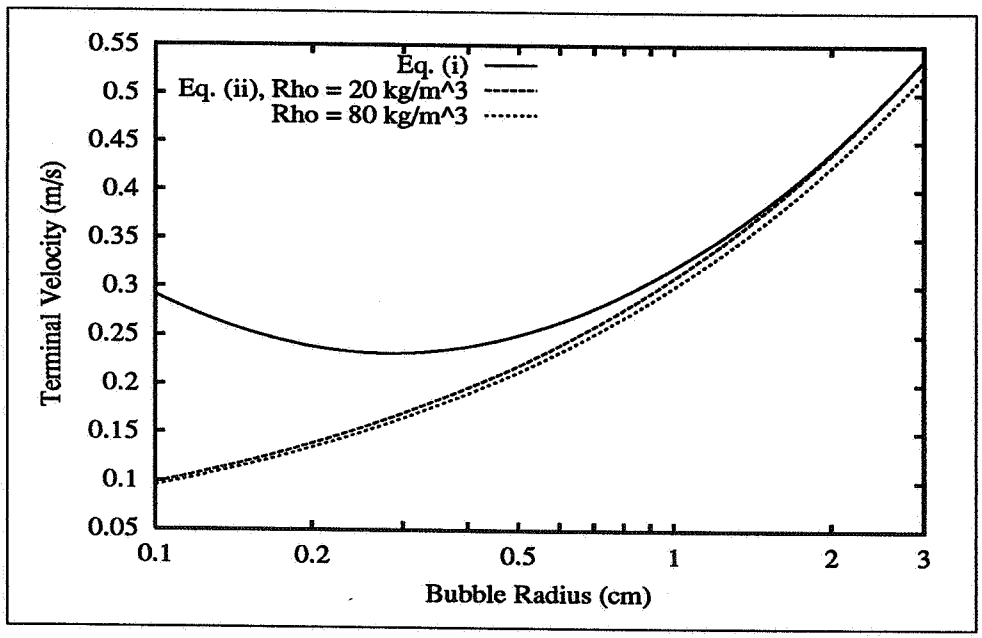

Figure 15: Terminal velocity of CO_2-bubbles in seawater. Eq. (i) is Eq. 41, and Eq. (ii) is Eq. 42.

The factor 0.98 in Eq. 41, which is added by us, ensures that the two expressions reach approximately the same value for large bubbles and for $\rho_{CO_2} = 20$ kg m^{-3}, see Fig. 15. U_T given by Eq. 41 is conservative in that it slightly overestimates the terminal velocity of CO_2-bubbles in water for $\rho_{CO_2} > 20$ kg m^{-3}. We have used Eq. 41 in our computations.

4.4 Mass Transfer Study of CO_2 Bubbles in Seawater

Diffusion can be described in two basic ways; by use of Fick's law and a diffusion coefficient, or by use of a mass transfer equation and a specified mass transfer coefficient. For bubbles in water — including CO_2-gas bubbles — there are mass transfer coefficients which provide quite accurate estimates of the diffusion process. We have therefore used a mass transfer approach in our bubble diffusion analysis.

If r (m) denotes the equivalent radius of the bubble, the mass transfer equation is given by the ordinary differential equation in time

$$\frac{d}{dt}\left(\frac{4}{3}\pi C_b r^3\right) = -4\pi r^2 k\,(C_s - C_\infty)\,. \tag{43}$$

In Eq. 43, k (m s^{-1}) is the mass transfer coefficient, C_b the concentration of CO_2-gas inside the bubble, and C_s and C_∞ the concentration of dissolved CO_2 at the surface and far away from the bubble, respectively. The CO_2 concentrations are given in moles m^{-3}. The value of C_s equals $[CO_2(aq)]$ in Henry's modified law (Eq. 25), whereas C_∞ is handled as a free parameter.

Eq. 43 can easily be solved for a prescribed value of C_b at time $t = 0$, and a prescribed mass transfer coefficient k. Numerical calculations based on boundary layer theory for bubbles in fluids give the following expression for k (Clift *et al.*, 1978):

$$k = \frac{2}{\sqrt{\pi}}\left(1 - \frac{2.89}{\sqrt{\mathrm{Re}}}\right)^{1/2}\sqrt{\frac{D_{CO_2} U_T}{2r}}\,. \tag{44}$$

In Eq. 44, D_{CO_2} is the diffusion coefficient for CO_2(g) in water, U_T is the terminal velocity of the bubble, and $\mathrm{Re} = 2\rho_w r U_T/\mu_w$ is the dimensionless Reynolds number. Eq. 44 approximates the mass transfer from bubbles in liquids for $\mathrm{Re} > 70$ (Clift *et al.*).

For seawater density $\rho_w = 1028$ kg m^{-3} at 35 pro mil salinity and for $T_c > 5$°C, we have that $\mathrm{Re} > 4000$ for $r \gtrsim 1$ cm. The expression in brackets in Eq. 44 is then close to unity. Calderbank *et al.*, 1970, with the unity approximation, have experimentally verified that the mass transfer from CO_2(g) bubbles in water follows Eq. 44 closely.

The diffusion coefficient for CO_2 in water, D_{CO_2}, is a well-known experimental determined quantity. For water at 25°C and at atmospheric pressure, we adopt the value (Tse and Sandall, 1979)

$$D_{CO_2} = 1.94 \times 10^{-9}\ \mathrm{m^2\ s^{-1}}\,. \tag{45}$$

For diffusion in liquids, the Stokes-Einstein relation (Lerman, 1979)

$$D_{CO_2}\mu_w/T = \text{const.}\,, \tag{46}$$

where T is temperature in Kelvin, can be used to extrapolate the value of D_{CO_2} to other temperatures and pressures.

The mass transfer equation for gas-bubbles in water, Eq. 43, can be put in the form

$$\frac{dr}{dt} = -k\frac{C_s - C_\infty}{C_b} - r\frac{U_T}{3\,C_b}\frac{dC_b}{dz}\,, \tag{47}$$

where we have used that

$$\frac{dC_b}{dt} = \frac{dC_b}{dz}\frac{dz}{dt} = U_T\frac{dC_b}{dz}\,.$$

The k-term in Eq. 47 gives the mass transfer of CO_2 out of the gas bubble (for $C_s > C_\infty$), whereas the dC_b/dz-term describes the effect of the compressibility of the CO_2-gas.

The dC_b/dz-factor in Eq. 47 can be expressed as a pure algebraic factor by means of an equation of state for the CO_2-gas and the hydrostatic pressure equation since

$$\frac{dC_b}{dz} = \frac{dC_b}{dP}\frac{dP}{dz}. \tag{48}$$

The equation of state for the CO_2-gas is taken as the modified van der Waals equation (Eq. 15)

$$P = \frac{RTC_b}{1 - bC_b} - aC_b^2, \tag{49}$$

with the parameters a and b given by (16). From Eq. 49, we have that

$$\frac{dC_b}{dP} = \frac{(1 - bC_b)^2}{RT - 2aC_b(1 - bC_b)^2}. \tag{50}$$

In the gaseous phase, $dC_b/dP > 0$.

To a high degree of accuracy, the hydrostatic equation can be taken as

$$P = P_0 - \rho_w g z \times 10^{-5}, \tag{51}$$

where P_0 (bar) represents the atmospheric pressure, g (m s^{-2}) is the gravitational acceleration, and the minus-sign reflects that z (m) is positive upwards.

Expression 48 can now be written as

$$\frac{dC_b}{dz} = -\frac{\rho_w g(1 - bC_b)^2}{RT - 2aC_b(1 - bC_b)^2} \times 10^{-5}. \tag{52}$$

The system of equations which govern the mass transfer of CO_2 from bubbles in seawater are given in Tab. 9. Eq. 43 has been solved numerically for $r(t)$ using a fourth order Runge-Kutta scheme (Cheney and Kincaid, 1985). The system has been solved in the following way: Initial bubble radius and depth are prescribed. The hydrostatic pressure corresponding to the given depth is computed from Eq. 51. At any instant, the pressure in the gas bubble has to balance the hydrostatic pressure. (The force due to the surface tension can safely be neglected for the bubbles we consider, i.e. for bubbles with $r \gtrsim 1$ mm). The equation of state of the CO_2 gas, Eq. 49, is then solved with respect to C_b. Furthermore, C_s is computed from Henry's modified law (Eq. 22), and the terminal velocity from Eq. 41. The right hand side of Eq. 43 is known since C_∞ is treated as a free parameter. Eq. 43 can now be stepped forward in time; from $t = t_0$ to $t = t_0 + \Delta t$, say, where Δt denotes the time step. During this timestep, the bubble has risen a distance $U_T \cdot \Delta t$. This gives us the new depth, which in turn give us the new hydrostatic pressure and the new C_b, and so on.

In the following paragraphs we describe different solutions of the bubble-system in Tab. 9.

4.4.1 Numerical Calculation of Pure Bubble Expansion in Seawater

The effect of the compressibility term in Eq. 47 can be seen by setting $k \equiv 0$ in the equation, i.e. neglecting the masss transfer. This situation simulates the evolution of r for a bubble with an inert gas in seawater, at least as long as the equation of state of the actual gas is not far away from Eq. 49. In Fig. 16, we have plotted the computed radius of the bubble as a function of depth. Largest radius in Fig. 16 is 3 cm, since bubbles in water are assumed to break-up for $r \gtrsim 3$ cm (Subsec. 4.2).

$\frac{dr}{dt}$	=	$-k\frac{C_s - C_\infty}{C_b} - r\frac{U_T}{3C_b}\frac{dC_b}{dz}$	Eq. 43
k	=	$\frac{2}{\sqrt{\pi}}\left(1 - \frac{2.89}{\sqrt{\mathrm{Re}}}\right)^{1/2}\sqrt{\frac{D_{CO_2}U_T}{2r}}$	Eq. 44
C_s	=	$K_0 f_{CO_2} \exp[(1-P)\bar{v}_{CO_2}/RT]$	Eq. 22
$\frac{dC_b}{dz}$	=	$-\frac{\rho_w g(1-bC_b)^2}{RT - 2aC_b(1-bC_b)^2} \times 10^{-5}$	Eq. 52
P	=	$P_0 - \rho_w g z \times 10^{-5}$	Eq. 51
P	=	$\frac{RTC_b}{1-bC_b} - aC_b^2$	Eq. 49
D_{CO_2}	:	Diffusion coefficient	Eqs. 45, 46
f_{CO_2}	:	Fugacity of CO_2	Eqs. 14, 18
K_0	:	Henry's law constant	Eq. 23
R	=	0.083144 bar L K^{-1} $mole^{-1}$	
Re	=	$2r\rho_w U_T/\mu_w$	Subsec. 4.1
ρ_w	:	Density of seawater, formula in UNESCO, 1981	Subsec. 3.7
U_T	:	Terminal velocity	Eq. 41
$\bar{v}_{CO_2}$	:	Partial molar volume of CO_2 in water	Subsec. 3.6

Table 9: Equations and quantities describing the mass transfer of CO_2 bubbles in seawater.

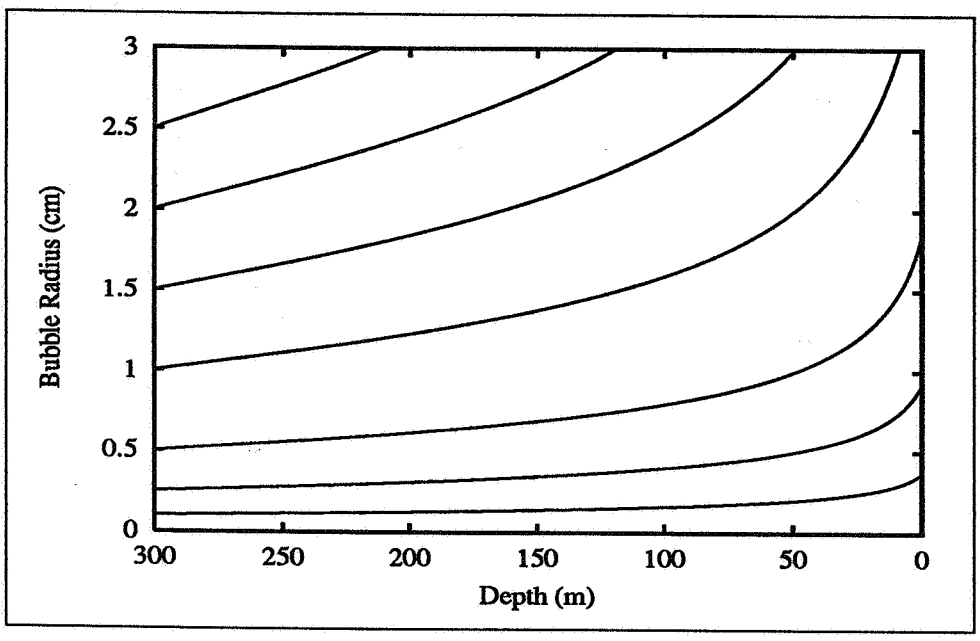

Figure 16: Bubble expansion for an artificial inert CO_2 gas in seawater at $T = 5°C$ and $S = 35$ pro mil. The bubbles are released at 300 metres depth with radii between 0.1 and 2.5 cm.

4.4.2 Mass Transfer vs Compressibility

Fig. 17 shows for which values of the bubble radii, depth and C_∞ the mass transfer and compressibility terms of Eq. 47 balance, i.e. when

$$k(C_s - C_\infty) = r\frac{U_T}{3}\frac{dC_b}{dz}, \tag{53}$$

where dC_b/dz is given by Eq. 52. From Eq. 47, we see that mass transfer term reduces r whereas the compressibility term increases r ($dC_b/dz < 0$).

The mass transfer term is greater than the compressibility term for values of r and depth below and to the left of the curves in Fig. 17. We see that the mass transfer term generally overcomes the compressibility term for depths greater than 100 meters and for low to moderate C_∞-values. Thus, in this parameter range, the radius of the bubble decreases continuously as the bubble ascends through the water column.

4.4.3 Bubble Diffusion with $C_\infty = 0$

In Figs. 18 and 19, we have plotted the number of moles of CO_2 gas in the bubble as function of depth. The bubbles are released at 50, 100, 200 and 300 metres, and the initial radii are 3, 2, 1 and 0.5 cm. It is seen that the largest bubbles released at shallow depths rise to the surface although some mass transfer is taking place. For the 2–300 metres release depths, the bubbles with $r(t = 0) \leq 2$ cm are totally dissolved after less than 80 metres ascent, the $r(t = 0) = 3$ cm bubbles rise a distance of up to 140 metres before all the initial CO_2 gas has been transfered out of the bubble. From Figs. 18 and 19 we see that for a given initial bubble

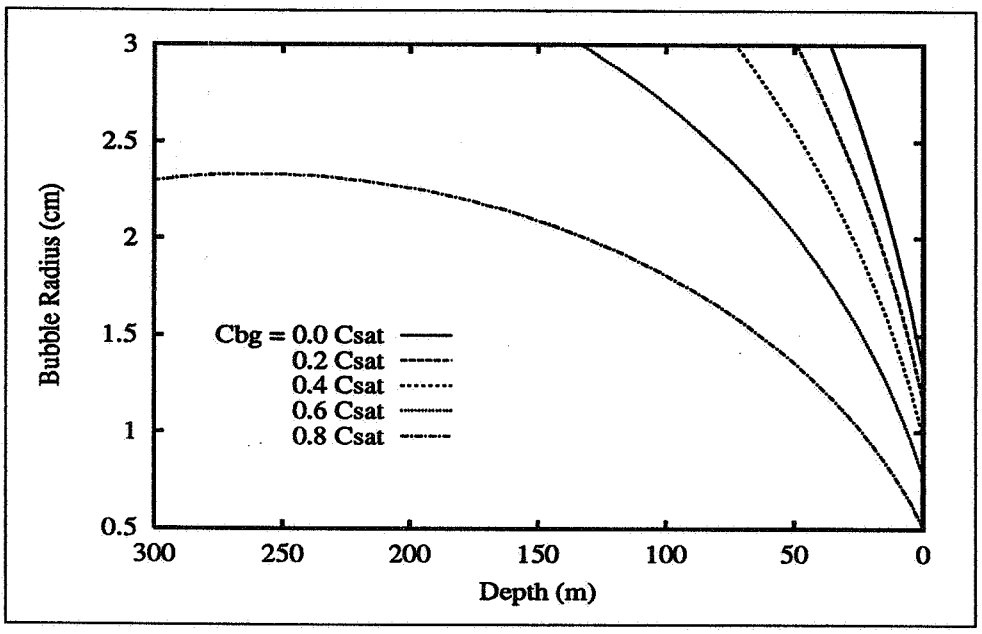

Figure 17: Contour plot of Eq. 53 for $T_c = 7°C$. The mass transfer term is the dominant term for values of r and depth below and to the left of the contours. **Cbg** and **Csat** are C_∞ and C_s, respectively.

radius, the initial number of moles of CO_2 gas inside the bubble increases with increasing release depth. This is, of course, a direct concequence of the equation of state of the CO_2 gas. A consecuence of this is that bubbles released at 300 metres ascend a longer distance than bubbles released at 200 metres.

The temperature effect is mainly due to the Henry's law constant; the solubility of CO_2(g) increases with decreasing temperature (Fig. 9). Therefore the magnitude of the mass transfer term in Eq. 43 increases with decreasing temperature.

Fig. 20 shows the results for the 200 and 300 metres release depths. The content of CO_2(g) in the bubbles are now normalized against the initial bubble CO_2(g) content. In this way the effect of different bubble radii is easily seen. The temperature 7°C represents a typical temperature for the oceanic waters off the Norwegian coast.

4.4.4 Bubble Diffusion with $C_\infty > 0$

So far we have considered the case $C_\infty = 0$. This means that the concentration of dissolved CO_2 in the vicinity of the bubble is negligible. For a high concentration ensemble of bubbles ascending through the water column, this is obviously not the case. The effect of non-zero background CO_2(aq) concentrations may be simulated by setting $C_\infty = \eta C_s$, where η is a number between 0 and 1. Figs. 21–23 show the normalized content of CO_2(g) in bubbles released at depths of 200 and 300 meters for various values of C_∞. The initial radii are 1, 2 and 3 cm.

The value of C_∞ is held constant through the entire bubble ascent.

For $r(t = 0) = 1.0$ cm, the effect of non-zero C_∞ is relatively small. In fact, the increase

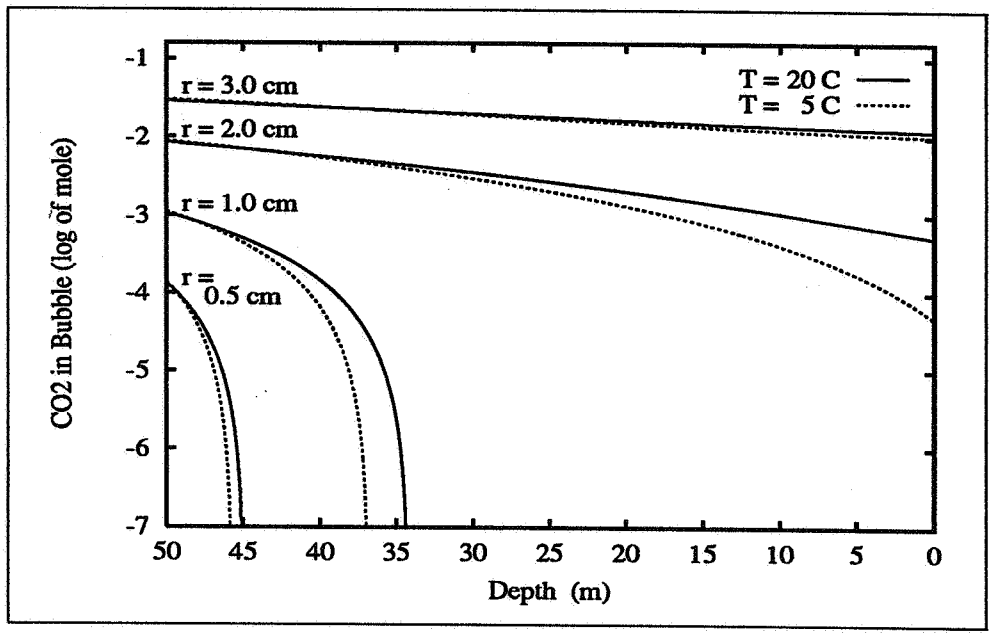

(a) Release depth 50 m.

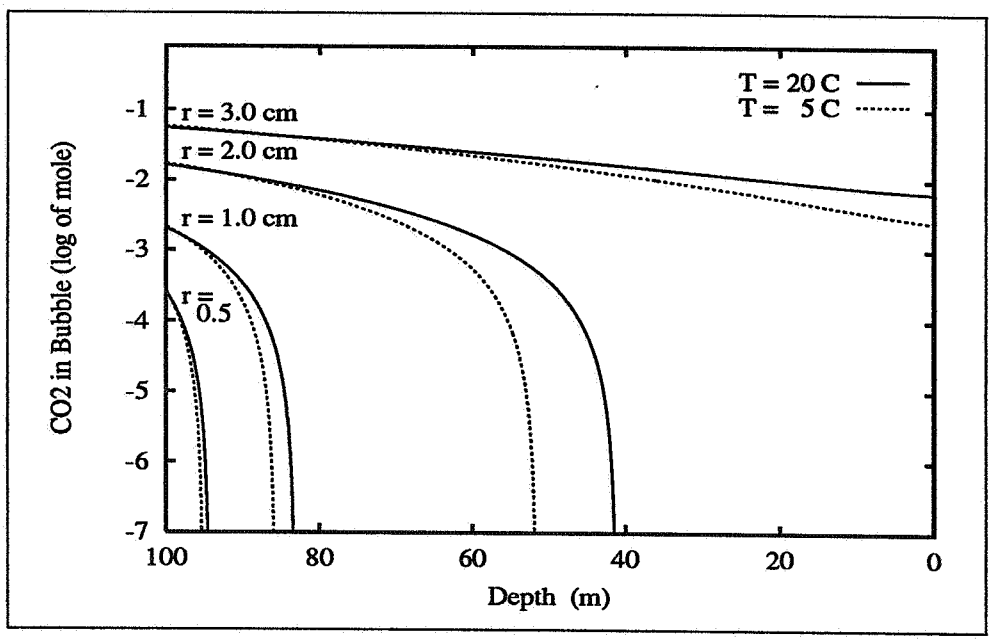

(b) Release depth 100 m.

Figure 18: The content of CO_2(g) in bubbles released at 50 and 100 m as a function of depth. Temperatures as indicated; $S = 35$ pro mil, and $C_\infty = 0$.

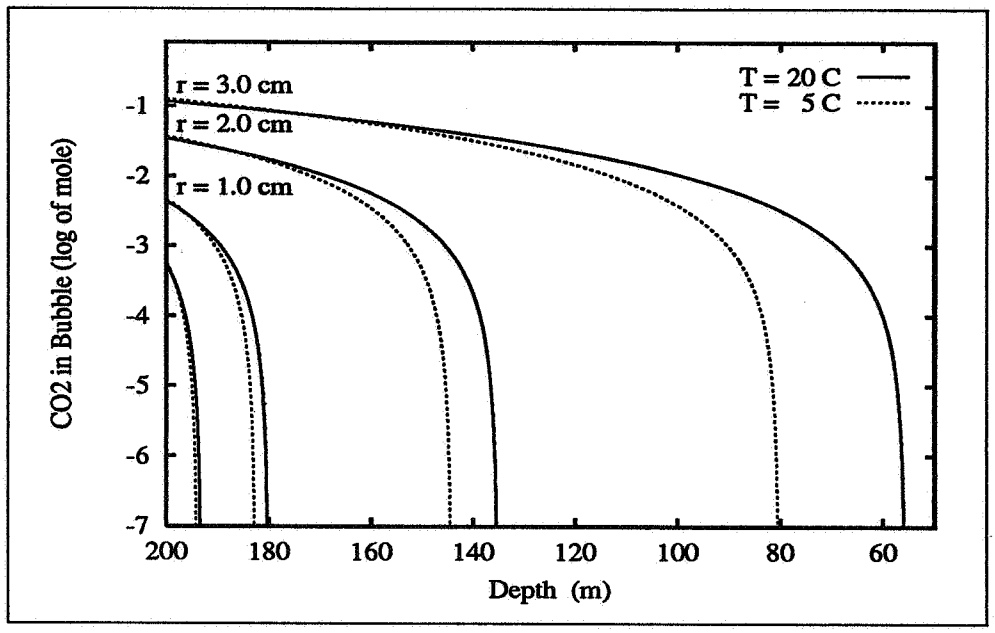

(a) Release depth 200 m.

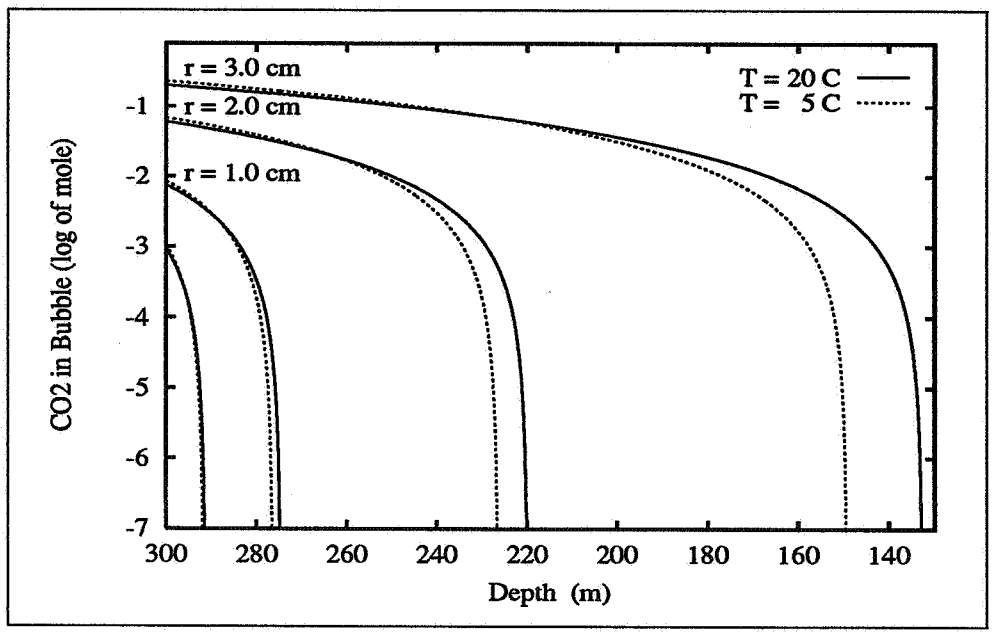

(b) Release depth 300 m.

Figure 19: The content of CO_2(g) in bubbles released at 200 and 300 m as a function of depth. Temperatures as indicated; $S = 35$ pro mil and $C_\infty = 0$. Initial radii are 3, 2, 1 and 0.5 cm.

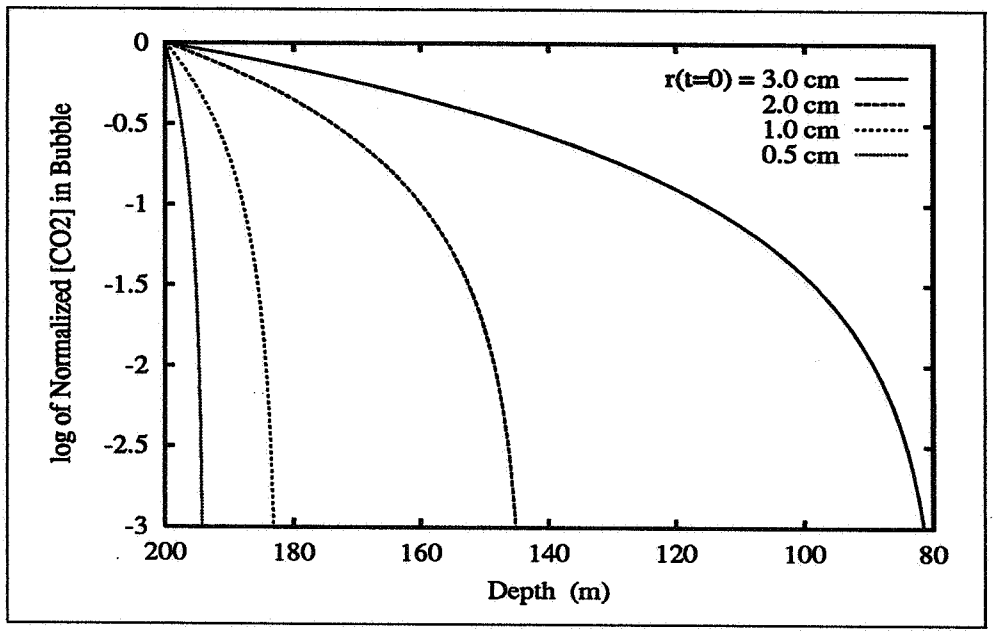

(a) Release depth 200 m.

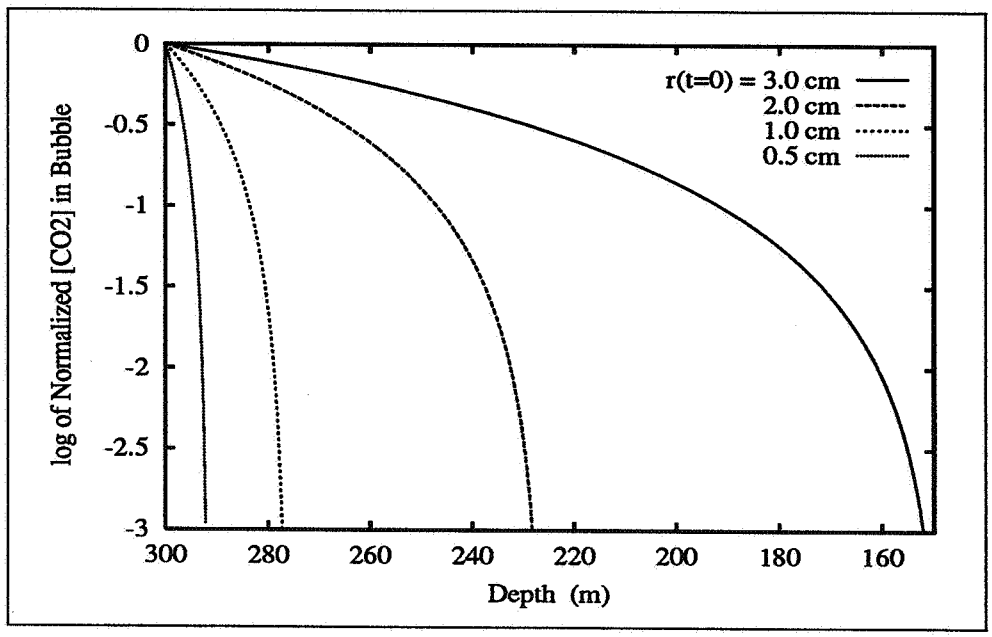

(b) Release depth 300 m.

Figure 20: Normalized content of CO_2(g) in bubbles released at 200 and 300 m. $T_c = 7°C$; $S = 35$ pro mil and $C_\infty = 0$.

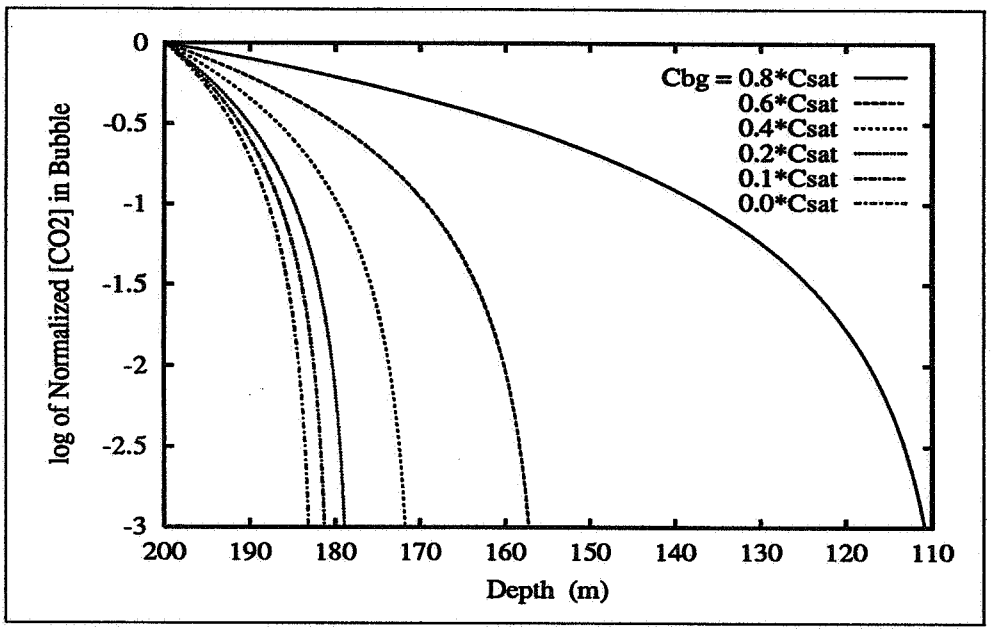

(a) Initial radius $r = 1.0$ cm.

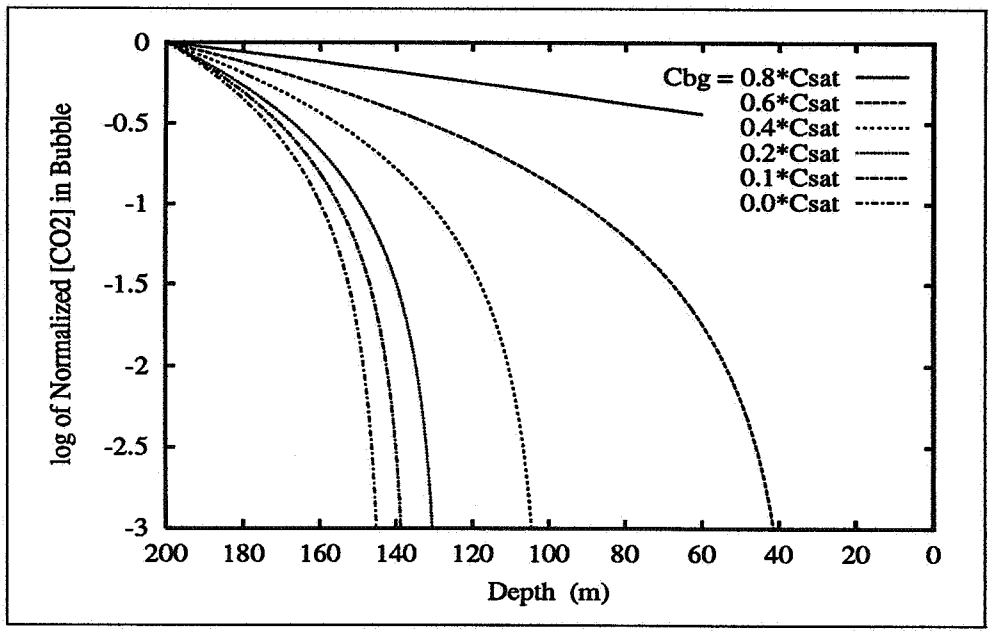

(b) Initial radius $r = 2.0$ cm.

Figure 21: Normalized content of CO_2(g) in bubbles released at 200 m for various values of C_∞ (named Cbg). Csat is C_s in Eq. 43. $T_c = 7°C$ and $S = 35$ pro mil.

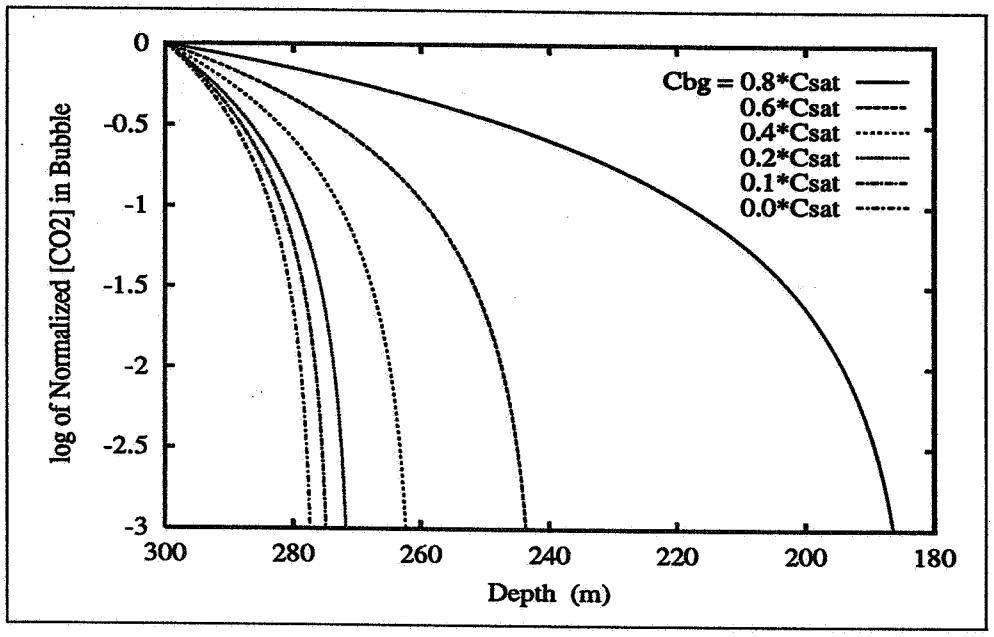

(a) Initial radius $r = 1.0$ cm.

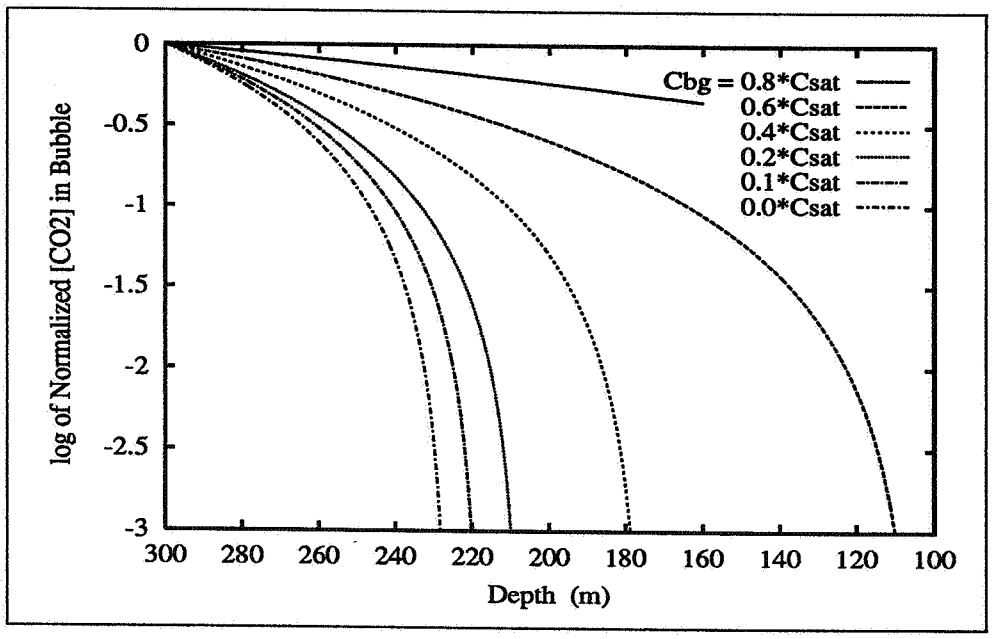

(b) Initial radius $r = 2.0$ cm.

Figure 22: Normalized content of CO_2(g) in bubbles released at 300 m for various values of C_∞ (named Cbg). Csat is C_s in Eq. 43. $T_c = 7°C$ and $S = 35$ pro mil.

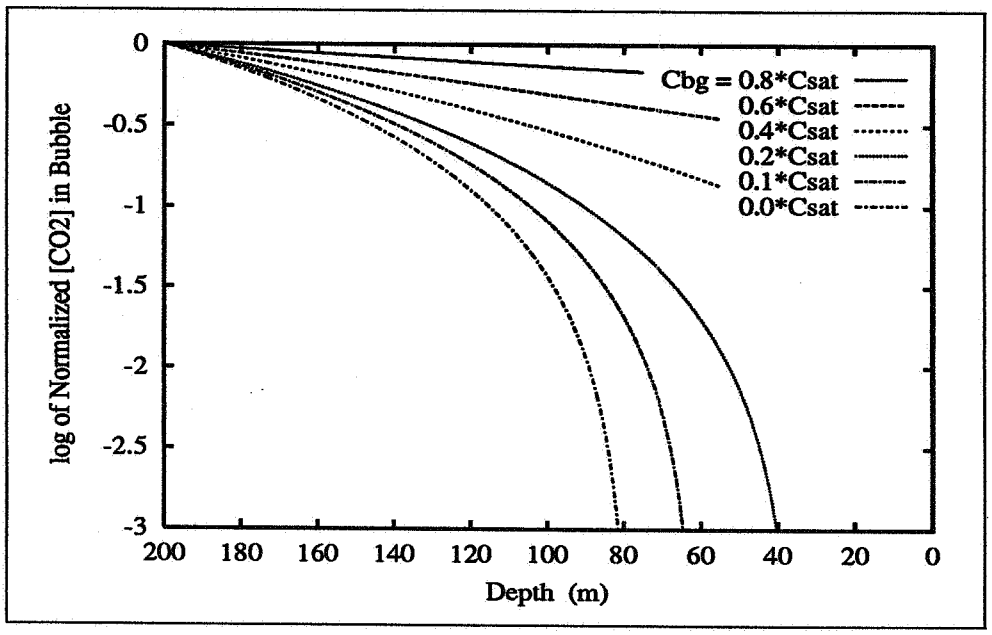

(a) Initial radius $r = 3.0$ cm.

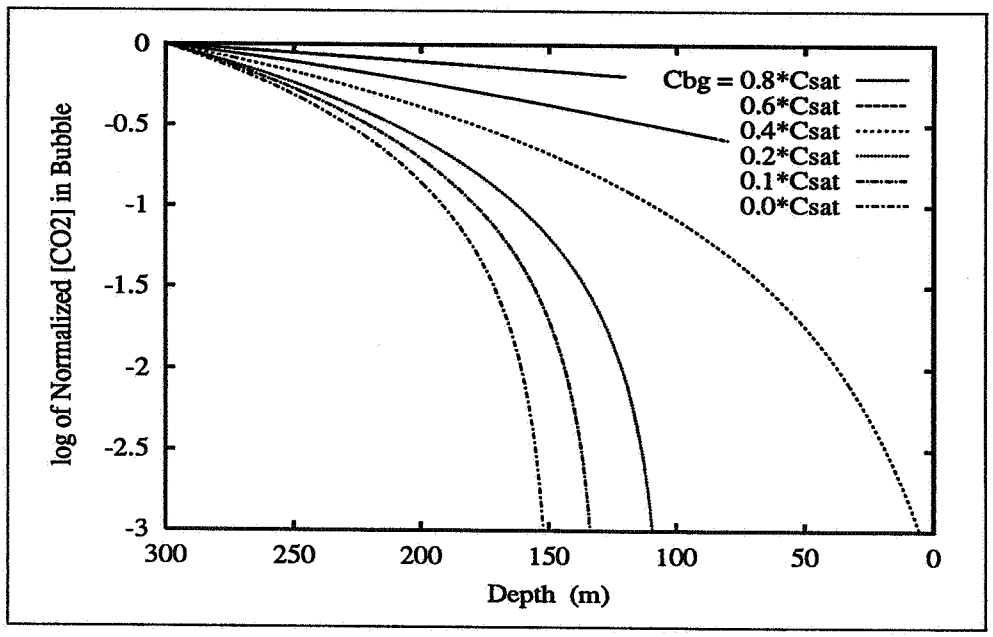

(b) Initial radius $r = 3.0$ cm.

Figure 23: Normalized content of CO_2(g) in bubbles released at 200 and 300 m for various values of C_∞ (named Cbg). Csat is C_s in Eq. 43. $T_c = 7°C$ and $S = 35$ pro mil.

in the ascending distances is less than 35 metres for $C_\infty \leq 0.6\,C_s$, and the case $C_\infty = 0.6\,C_s$ is indeed extreme.

For $r(t=0) = 2.0$ cm, $C_\infty \leq 0.2\,C_s$ only slightly reduces the transfer of CO_2 out of the bubbles. For $C_\infty \geq 0.4\,C_s$, the reduction in the mass transfer becomes appreciable.

For $r(t=0) = 3.0$ cm, $C_\infty \leq 0.2\,C_s$ increases the ascending distance less than 40 meters compared with $C_\infty = 0$. Higher concentrations of C_∞ can not be allowed, since then the bubbles will reach, or nearly reach, the surface of the ocean.

It should here be mentioned that the assumption $C_\infty = \text{const.}$ all the way through the water column is a very conservative assumption. If $CO_2(g)$ is injected into the ocean, only the water masses in the vicinity of the injection site will be saturated with respect to $CO_2(aq)$. This means that the bubbles will rise only 10–20 metres or so in relatively high C_∞ water masses, before C_∞ goes to zero. The vertical profile of C_∞ depends, of course, on the oceanic currents, mixing, turbulence, etc. at the injection site.

4.5 Summary

CO_2 bubbles should be released at a depth of 200 metres ore more in order to obtain complete dissolution before the uppermost 100 metres of the ocean is reached. Highly $CO_2(aq)$-enriched waters are expected to occur in the vicinity of the injection site. A background concentration of 0.2 to 0.3 times the saturation value of $CO_2(aq)$ has little effect on the mass transfer of CO_2 from the bubbles. We therefore conclude that bubbles released at 200 metres or more will be nearly totally dissolved after less than 100 metres ascent.

5 Oceanographic Conditions with Emphasis on the Coast of Norway

In this section the fate of injected carbon after the initial dissolution is discussed. The unfavorable case of CO_2 at low concentrations and in contact with the ocean surface is considered first. Then we discuss the competition between the negative buoyancy as described in Secs. 3 and 4, and mixing processes which will dilute the plume from an injection point. Finally we consider applicability of the injection method along the coast of Norway.

5.1 Outgassing from Enriched Water in Contact with the Ocean Surface

To compute the fate of injected carbon, we generally have to solve a mass conservation equation for carbon, including a source at the injection site, advection and diffusion due to ocean currents and mixing processes, and exchange with the atmosphere due to changes in near surface partial pressure of CO_2. The alkalinity and the rate of biological conversion of dissolved carbon into sinking matter is assumed to be unaffected by the injected CO_2.

A very simple case which will be considered is when the injected carbon occurs in so low concentrations that the density effect studied in Sec. 3 may be neglected, and when oceanographic conditions are such that the injected carbon may be assumed to rapidly spread evenly in the vertical all the way from the ocean bottom to the surface. This will obviously be a pessimistic case with regard to outgassing, but in cases of strong vertical mixing such as in southern and western parts of the North Sea, and also during strong winter time mixing further north along the coast, it may not be totally unrealistic.

The conservation equation may conveniently be formulated in terms of only perturbation total carbon concentration δC_T, i.e. actual C_T minus the background value of C_T. This means we are computing only the concentration of "tagged" carbon from the injection site. The possible outgassing of tagged CO_2 that is computed must be interpreted as a modification of the background outgassing/uptake.

If the water depth is denoted H (m) and the perturbation of total carbon concentration C (mole m^{-3}) is confined to a horizontal area A (m^2) which may vary in time, the following equation applies for a certain amount of injected carbon:

$$\frac{d}{dt}(AHC) = -AFC\,, \tag{54}$$

where F (m $year^{-1}$) is an air-sea gas transfer coefficient for carbon written in terms of total carbon concentration and including the buffering effect in seawater. The equation describes the conservation of injected carbon in seawater when the only sink of this carbon is due to air-sea exchange.

The increase in atmospheric pCO_2 due to outgassed CO_2 has been neglected here since the lateral mixing in the atmosphere is very much faster than in the ocean. CO_2 outgassed to the atmosphere would spread all over the globe in a few years and thus contribute to very little change of pCO_2 above an outgassing area which covers only a very small part of the earths surface. However, for injection of very large amounts, or for long term (order 1000 years) calculations, this effect would have to be included, since it is this effect which provides the equilibrium distribution of carbon between the atmosphere and the oceans in the absence of sediment interaction (Appendix A).

When H is constant, the above equation may easily be solved for the total perturbation of carbon content in the ocean:

$$(AHC)(t) = (AHC)_0 \exp[-(F/H)t], \tag{55}$$

where t is time and $(AHC)_0$ is the initial amount (number of moles) of carbon injected. This shows that the outgassing to the atmosphere occurs on a time scale of the order H/F.

Our gas-transfer coefficient F (m year^{-1}) is given by

$$F = E \frac{\partial p\mathrm{CO}_2}{\partial C_T}, \tag{56}$$

where E (mole m^{-2} year^{-1} μatm^{-1}) is the CO_2 exchange coefficient as given e.g. by Etcheto *et al.*, 1991, and $\partial p\mathrm{CO}_2/\partial C_T$ (m^3 atm mole^{-1}) represents the inorganic carbon buffering discussed in Sec. A.3.

With a seawater density of 1028 kg m^{-3}, and a partial pressure of atmospheric CO_2 of 360 μatm, we have from Fig. 26(a) that $\partial p\mathrm{CO}_2/\partial C_T$ is about 2.6×10^{-3} m^3 atm mole^{-1} for $T \approx 0$°C, and 2.1×10^{-3} m^3 atm mole^{-1} for $T \approx 10$°C. E varies seasonally and geographically mainly as a function of wind speed. From Etcheto *et al.*, 1991, its global mean value is of the order 0.03 mole m^{-2} year^{-1} μatm^{-1} with monthly mean values up to about 0.1 mole m^{-2} year^{-1} μatm^{-1} to be expected in winter time along the coast of Norway. For temperatures between 0 and 10°C, we get

$$F = 60\text{–}260 \text{ m year}^{-1}. \tag{57}$$

For a water depth of 300 metres, this gives a time scale H/F of 1–5 years. An outgassing of as much as $(1 - 1/e)$ of the injected carbon on such a rapid time scale is obviously not satisfactory for a CO_2 injection scheme. Outgassing will be even faster in shallower water. An increase in water depth does not give a sufficient lengthening of the time scale if we stick to this simple model which assumes rapid vertical mixing in the water column.

It is obvious from this calculation that additional physical mechanisms need to be invoked in order to obtain significantly longer residence times in the ocean. Lateral dilution is not critical since outgassing is proportional to the areally integrated perturbation in surface concentration. The areal distribution of this perturbation thus has no effect on the total outgassing. However, strong density stratification that would inhibit vertical mixing and thus keep injected CO_2 away from the surface would obviously be important. This requires consideration of regional oceanographic conditions and modelling of vertical mixing and diffusion processes. We return to this point in Sec. 5.3.

Vertical advection by sinking currents as suggested by Marchetti, 1977, or driven by the density effect studied in Sec. 3 are two possible mechanisms which would not only slow down the vertical transport towards the surface, but actively keep injected CO_2 down. This is discussed next.

5.2 The Fate of CO_2 Dissolved at High Concentration

In Sec. 4 dissolution from single bubbles was studied. Influence from other bubbles was only included via sensitivity studies of reduced dissolution due to increased carbon content in the surrounding water. The region close to the injection point where gas bubbles exist, may be called the bubble zone. In the case of injection of seawater which has previously been enriched with CO_2, no bubble zone is expected. In both cases however, the combined

sinking, spreading and dilution of the high carbon concentrations expected near the injection point will depend on ambient water currents and density stratification in the area as well as the initial buoyancy and momentum of the injected fluid.

The effect of initial momentum should be taken into account in the near field of the release point, definitely in the case of injection of enriched water and possibly also for injection of CO_2 in the gas phase. In the case of gas injection, the contribution from gas momentum out of the pipe to the velocity of enriched water will be given by the mass fraction of CO_2 in enriched water multiplied by the gas velocity out of the pipe. The mass fraction may be up to 5% at maximum dissolution (Sec. 3). If the gas velocity out of the pipe, determined by the pumping capacity and pipe diameter, is several m s^{-1}, then the initial momentum of the gas flow may contribute to a speed of several cm s^{-1} of the enriched water. In the case of a pipe pointing downwards or downslope along the bottom, this will contribute to keeping the injected gas and thus the enriched water down.

Hydrodynamical plume models exist and may be directly applied to the injection of enriched water, given pipe diameter and pumping rate in addition to the initial concentration and the ambient currents and stratification (Lee, 1980). The gas injection case is more complicated since the effective source of buoyancy and momentum will be spread over a bubble zone, the extent of which has to be calculated as part of the problem. However, the extent of the bubble zone is expected to be limited (Sec. 4), so even if the mixing may increase in this case, the performance of a gas injection scheme may be almost as good as that of a scheme with injection of artificially enriched water. Further studies of this may be done based on given design parameters of the injection facilities.

If injection is performed close to the bottom in shallow water, this will have a beneficial effect in reducing the mixing with ambient water compared to injection at a similar depth in the deep ocean where an injected plume will spread laterally in all directions. In particular, a sloping bottom towards the deep ocean could act as a conduit leading the dense water efficiently to its level of neutral buoyancy with minimal entrainment of surrounding water. Studies of such bottom gravity currents could be based on the established models of Turner, 1973, Turner, 1981, Smith, 1975, and Killworth, 1977.

The dissolution of CO_2 at production rates similar to those of a single 1 GW gas power plant corresponds to rather small water fluxes (Sec. 3) by oceanographic standards. Small scale canyons in the shelf slope, down to widths of the order 50 metres or less may thus be utilized to limit lateral mixing of enriched water providing a safe and efficient gateway to the deep ocean. Such canyons may exist in many places on the continental shelf slopes of the world ocean. On the other hand, it might also be sufficient to simply inject carbon down a smooth continental slope. Mixing will then depend on the regional stratification and currents including the rapidly varying part of the currents such as tides, internal waves and eddies.

If enriched water contacts $CaCO_3$-containing sediments, enhanced dissolution may occur, leading to accelerated sequestration. The rates involved in this process are poorly known (Broecker and Peng, 1982), in particular the effects of high carbon concentrations such as may be expected in an enriched bottom plume or gravity current. The effect is anyway thought to be small at shallow depths near Norway where the fraction of calcium in bottom sediments is normally low. It might however provide a positive effect when the plume has reached greater depths.

One uncertainty about CO_2 injection is the rate of hydrate formation. Heavy hydrates may form and sink to the bottom both close to the injection point and later along the path of a bottom gravity current. While formation at the injection site may be avoided by choosing

injection conditions below the hydrate line in Fig. 7, we do not know to what extent hydrates will form later on. Hydrate formation may in itself be considered a method for efficient disposal of CO_2 on the sea bottom and thus be advantageous. However, the environmental impact may be severe, particularly for marine life near bottom. This has to be investigated. At least spawning grounds for various fish species should be avoided.

5.3 Large Scale Oceanographic Conditions Along the Coast of Norway

The large scale surface current and front system around Norway is shown in Fig. 24. Deep

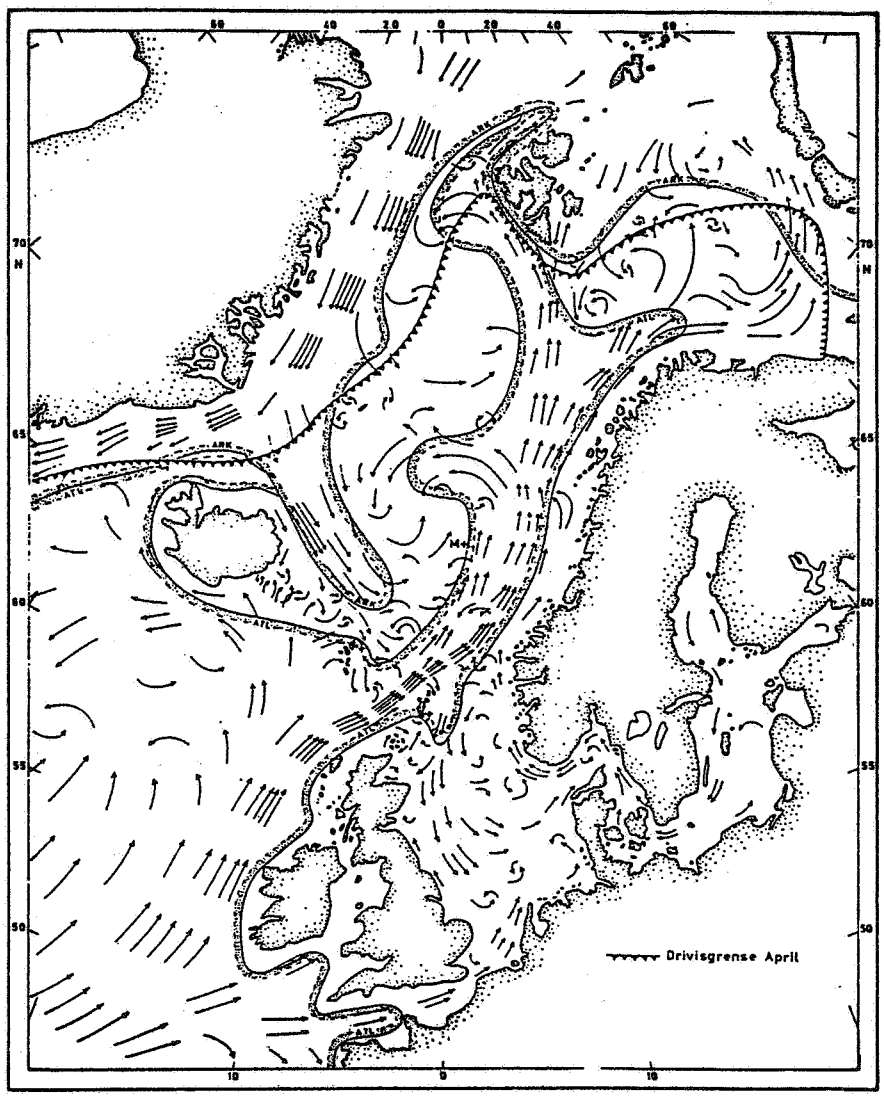

Figure 24: Ocean surface currents and fronts in the Nordic Seas. From Mosby, 1977.

water formation in the Greenland Sea is thought to be one major driver of this circulation. Intermediate and deep water in the Greenland-Norwegian Sea is transported southward beneath the surface currents across the Greenland-Scotland ridge towards the North Atlantic

and plays an important role in the deep circulation of the world oceans. These water masses will stay in the deep ocean for a period of the order 1000 years before upwelling in the Pacific and Indian Oceans.

A discussion of regional aspects relevant to CO_2 injection along the coast of Norway as well as large scale mixing process is given in our report to SFT (Haugan and Drange, 1991). We note here that such discussion is particularly important for diluted CO_2, i.e. that part of the injected amount which does not take part in deep sinking associated with a bottom gravity current. A few additional comments are in order here.

Holt and Lindeberg, 1990, recommended a location near Ålesund because here depths of more than 500 metres could be reached within 93 km of the shore. However, this is an area where the Norwegian Atlantic current which comes along the shelf break from the south, splits into two branches, one of which climbs onto the shelf towards the Haltenbank area. Oceanographic measurement campaigns in this area in winter 1988 (Haugan *et al.*, 1991) and in late fall 1991 (*NORCSEX* 1991, J.A. Johannessen, personal comm.) have demonstrated the strength of this upslope current which is likely to transport large portions of injected CO_2 onto the shelf giving rapid outgassing (section 5.1). This location should therefore not be recommended. First of all, strong and unfavorable currents such as in this area should be avoided, and secondly a more gently sloping shelf break would be beneficial in limiting the dilution of the enriched water.

The almost vertically homogeneous southern and western North Sea is obviously not a good choice. In the Barents Sea rapid vertical mixing is expected during winter time surface cooling. However the western part dipping towards the Norwegian Sea or the Bear Island Channel may be worthy of further study.

It may also be that segregation of enriched water close to the bottom is sufficiently strong to keep injected CO_2 away from the surface by itself. Saline water produced by ice freezing in the north-eastern Barents Sea in winter has been observed to collect near bottom and fill up topographic depressions and is believed to be transported towards the Arctic Ocean east of Frans Josef Land (Midttun, 1985). The excess density due to increased salinity in these cases is small in comparison to the excess density that may result from CO_2 enrichment. This indicates that injection may work even in homogeneous water.

More favorable locations may be found along the coast of Troms, where the access to the Norwegian Sea should be direct and unproblematic.

The west coast from about 60 to 62° N may also be a good location. Here 300 m water depth may be found very close to the coast, and the northward sloping Norwegian Trench with the northward flowing current underneath a stratified surface layer should help steering enriched water towards the Norwegian Sea (Haugan and Drange, 1992).

In general, the fate of carbon diluted into low concentrations is probably not as pessimistic as indicated in section 5.1. The most severe limiting factor for estimating this better is the present knowledge of vertical mixing processes in the ocean as expressed by vertical diffusivity coefficients. Estimates from measurements of various tracer distributions exist, and may be used in modelling studies.

However, if injection can be carried out in such a way that most of the carbon is maintained at high concentrations close to the bottom until reaching great depths, this is obviously a much safer method which presently looks very promising.

6 Conclusions

The oceans are estimated to be able to ultimately take up 85 - 95% of the CO_2 emitted to the atmosphere due to burning of fossil fuels, possibly less if the ocean circulation pattern changes as a result of increased greenhouse effect. The rate of uptake is however much slower than the present emission rates, and the fractional uptake is steadily decreasing as the atmospheric CO_2 content increases. A significant transient maximum in atmospheric CO_2 content during the period of fossil fuel burning is therefore expected.

Successful injection of CO_2 in the ocean will reduce or remove the expected transient maximum in atmospheric CO_2 concentrations compared to the case of continued emissions to the atmosphere. However, on a time scale of several thousand years, injected CO_2 may be partitioned between the atmosphere, the oceans and the sediments in the same way as CO_2 emitted to the atmosphere. Injection is therefore not equivalent to reduced total burning in the long run, but it will reduce the maximum perturbation of the climate system and thereby reduce the probability of dramatic climate changes.

In order to obtain successful sequestration in the deep ocean, injection at large depths or in sinking currents has been proposed. Published studies demonstrate that the carrying capacity of the deep oceans such as the North Atlantic is sufficient to sequester a very large portion of the expected emissions.

We demonstrate in this study that also injection at shallow depths (200 - 300 m) may work well. The increase in seawater density due to dissolved CO_2 is significant and will contribute to sinking of CO_2-enriched water near the injection point.

Shallow injection may be carried out by pumping CO_2 in the gas phase to the release depth, where we demonstrate that dissolution will be rapid enough to ensure a significant carbon concentration and thus density increase. Alternatively, CO_2 may be dissolved in seawater at elevated pressure, and the enriched water pumped to the release depth. In either case, the release point should ideally be located near a sloping bottom which can lead the enriched water to great depths with minimum dilution from ambient water.

Several locations relatively close to the coast of Norway should be well suited for injection leading to long term sequestration in the Norwegian Sea. However, before injection in the ocean can be recommended, the theoretical predictions presented here should be verified, and possible environmental damage near the injection point should be investigated. Based on this preliminary study we believe the following points will be most important in further studies:

1. Uptake at the injection point addressing the issues of bubble stability and bubble interaction and including measurements of fundamental physical-chemical properties.

2. Mixing and dilution of CO_2-enriched water near the injection point addressing the issues of entrainment and buoyancy effects and including theoretical and possibly laboratory hydrodynamical studies.

3. Vertical mixing and outgassing of that part of the injected CO_2 which may escape from the heavy near bottom plume, including field work with tracers as well as testing and verification of numerical turbulence models.

4. Biological impact studies by tank experiments exposing various organisms to increased CO_2 levels.

5. Long range transport of injected CO_2 including both detailed studies of the enriched near bottom layer and large scale climate modelling.

With a focussed effort on these points, it should be possible to document sufficiently well for international acceptance whether the method has the potential that we presently believe, and what the impact on the environment will be.

Realizing that society may not be able to reduce the burning of fossil fuel sufficiently to obtain the desired reduction in atmospheric build-up of CO_2, the method seems very promising as a means to dispose of additional CO_2 and thus reduce the maximum expected greenhouse forcing.

A Some Theoretical Quantities and Concepts

In this appendix we will enlighten the reported results in Sec. 2 by some theoretical quantities. But first some words about CO_2 emissions and the atmospheric CO_2 content.

A.1 Fossil Fuel and Atmospheric CO_2

The atmospheric CO_2 content is normally given as mole fraction in units of parts per million on a volume basis (ppmv, or simply ppm). With a total atmospheric mass of 5.136×10^{18} kg, and a molecular weight of dry air of 28.9, the following conversion factor is easily derived (Kratz, 1985):

$$1 \text{ ppm } CO_2 \approx 2.13 \text{ Gt C}. \tag{58}$$

The preindustrial (i.e. before 1850) pCO_2 value is usually taken as 280 ppm. This means that the preindustrial atmosphere contained about 596 Gt C. The pCO_2 value for the present atmosphere is ca. 360 ppm, corresponding to 767 Gt C.

This year slightly more than 6 Gt C will be released to the atmosphere as a result of fossil fuel burning, cement manufacturing, and gas flaring. The total emissions of CO_2 on the Norwegian sector of the North Sea is 6.3 Mt C. The emissions are distributed between gas flaring (1.4 Mt C), use of CO_2 in turbins (4.6 Mt C) and use of diesel (0.3 Mt C) (B. Nordby, Norwegian State Pollution Authority, personal comm.).

The recoverable fossil fuel reserves re reported to be about 7100 Gt C (Hoffert *et al.*, 1979, and 4200 Gt C (Broecker and Peng, 1982).

A.2 Keeling Fraction

Significant amounts of atmospheric CO_2 enter the ocean water only because of the reaction

$$H_2O + CO_2(aq) + CO_3^{2-} \rightleftharpoons 2HCO_3^- , \tag{59}$$

derived from reactions (3) and (4) on page 6. Although the oceanic waters and sediments have the capacity to neutralize the amount of carbon locked up in the fossil fuel reserves, only a fraction of the atmospheric CO_2 will be neutralized before a new equilibrium between the atmosphere, ocean and sediment reservoirs is achieved.

Let us first consider an equilibrium between the atmosphere and the oceanic waters, and ignore the sediments. The expressions and reactions representing this system is given in Tab. 10. Eq. 60 in Tab. 10 is the definition of the Keeling fraction f_K (Broecker and Peng, 1982), and M_{atm} and M_{sea} are the fossil fuel CO_2 accumulated in the air and the ocean, respectively. Neglecting non-anthropogenic sinks and sources for the atmospheric CO_2 content, M_{atm} is given by Eq. 61, where p^0CO_2 and M^0_{atm} represent the preindustrial partial pressure and mass of CO_2 in the air. Correspondingly, the oceanic CO_2 content is given by Eq. 62, where C^0_T and M^0_{sea} are the preindustrial inorganic carbon content and mass, respectively. M_{ff} is the total amount of emitted fossil fuel CO_2; $M_{\text{ff}} = M_{\text{atm}} + M_{\text{sea}}$. The other expressions in Tab. 10 are defined in Subsec 3.1, with the following comment: The alkalinity A is set constant, which is a reasonable assumption as long as dissolution of the calcium carbonate sediments is neglected (see below).

The expressions below the line in Tab. 10 can be combined into a single equation:

$$A = \frac{K_0 K_1'}{[H^+]} pCO_2 + 2\frac{K_0 K_1' K_2'}{[H^+]^2} pCO_2 + \frac{K_B' B_T}{[H^+] + K_B'} + \frac{K_W'}{[H^+]} - [H^+]. \tag{64}$$

$$f_K = \frac{M_{\text{atm}}}{M_{\text{atm}} + M_{\text{sea}}} \tag{60}$$

$$M_{\text{atm}} = \frac{p\text{CO}_2 - p^0\text{CO}_2}{p^0\text{CO}_2} M^0_{\text{atm}} \tag{61}$$

$$M_{\text{sea}} = \frac{C_T - C^0_T}{C^0_T} M^0_{\text{sea}} \tag{62}$$

$$M_{\text{ff}} = \frac{p\text{CO}_2 - p^0\text{CO}_2}{p^0\text{CO}_2} \frac{M^0_{\text{atm}}}{f_K} \tag{63}$$

$[\text{CO}_2(\text{aq})] = K_0\, p\text{CO}_2$	Eq. 22
$K'_1 = \dfrac{[\text{HCO}_3^-][\text{H}^+]}{[\text{CO}_2(\text{aq})]}$	Eq. 3
$K'_2 = \dfrac{[\text{CO}_3^{2-}][\text{H}^+]}{[\text{HCO}_3^-]}$	Eq. 4
$K'_B = \dfrac{[\text{B(OH)}_4^-][\text{H}^+]}{[\text{B(OH)}_3]}$	Eq. 8
$K'_w = [\text{H}^+][\text{OH}^-]$	Eq. 11
$C_T = [\text{CO}_2(\text{aq})] + [\text{HCO}_3^-] + [\text{CO}_3^{2-}]$	Eq. 5
$B_T = [\text{B(OH)}_3] + [\text{B(OH)}_4^-] = (S/35) \cdot 4.106 \times 10^{-4}$	Eqs. 9–10
$A = [\text{HCO}_3^-] + 2[\text{CO}_3^{2-}] + [\text{B(OH)}_4^-] + [\text{OH}^-] - [\text{H}^+] = \text{const.}$	Eq. 7

Table 10: The system of expressions and reactions governing the equilibrium state between the atmosphere and ocean. The expressions above the line are explained in the text, those below the line are given in Subsec. 3.1. Numerical values of the equilibrium constants are found in UNESCO, 1987.

For constant A and prescribed pCO_2, Eq. 64 can be solved for $[H^+]$. C_T can then be determined from the expression

$$C_T = K_0 \left(1 + \frac{K_1'}{[H^+]} + \frac{K_1' K_2'}{[H^+]^2}\right) pCO_2 , \tag{65}$$

which in turn determines the Keeling fraction f_K. Eq. 65 is found by combining the expressions for K_1', K_2', C_T and $[CO_2(aq)]$ in Tab. 10. We have followed Broecker and Peng, 1982, and divided the ocean into subvolumes after the water temperature. Broecker and

Temperature (°C)	Volume 10^{16} m^3	Volume Fraction	C_T^0 (mmole kg^{-1})	M_{sea}^0 (10^{16} mole)
> 24	1.0	0.008	1.938	1.992
20–24	0.7	0.005	1.975	1.421
16–20	1.7	0.013	2.012	3.516
12–16	2.7	0.020	2.048	5.684
8–12	3.3	0.025	2.081	7.060
4–8	14.9	0.113	2.112	32.35
2–4	55.0	0.417	2.139	120.9
1.5–2	11.6	0.087	2.139	25.51
1–1.5	24.5	0.186	2.139	53.84
0–1	13.2	0.100	2.139	29.03
< 0	3.4	0.026	2.139	7.476
Total	132.0	1.000		

Table 11: Subdivison of the ocean after temperature. Data from Broecker and Peng, 1982, and Worthington, 1981.

Peng use one single subvolume for temperatures below 4°C, and this subvolume constitutes about 82% of the total oceanic volume. Such a large volume might be critical, especially since cold waters are able to store more CO_2 than warmer waters. We have therefore divided the $T_c < 4$°C volume into 5 subvolumes. Tab. 11 gives relevant physical and chemical properties of each of the volumes. Furthermore, we use the values

$$M_{atm}^0 = 5 \times 10^{16} \text{ mole} \quad \text{and} \quad p^0CO_2 = 280 \times 10^{-6} \text{ atm}$$

(Broecker and Peng, 1982). f_K and M_{atm}/M_{atm}^0 for equilibrium between the ocean waters and atmosphere are shown as solid curves in Fig. 25. The dotted curves in Fig. 25 represent equilibrium between the ocean waters, sediments and atmosphere. The curves have been plotted to the point where $M_{ff} = 12\, M_{atm}^0$, since this number might be taken as an estimate of the recoverable fossil fuel reserve of 7200 Gt C. The principal reaction describing the dissolution of calcium carbonate sediments is

$$H_2O + CO_2 + CaCO_3 \rightleftharpoons Ca^{2+} + 2HCO_3^- . \tag{66}$$

We see that when the CO_2 content of the oceanic water increases, parts of the CO_2 ends up as HCO_3^-, this is the calcium carbonate buffering. From the definition of the alkalinity

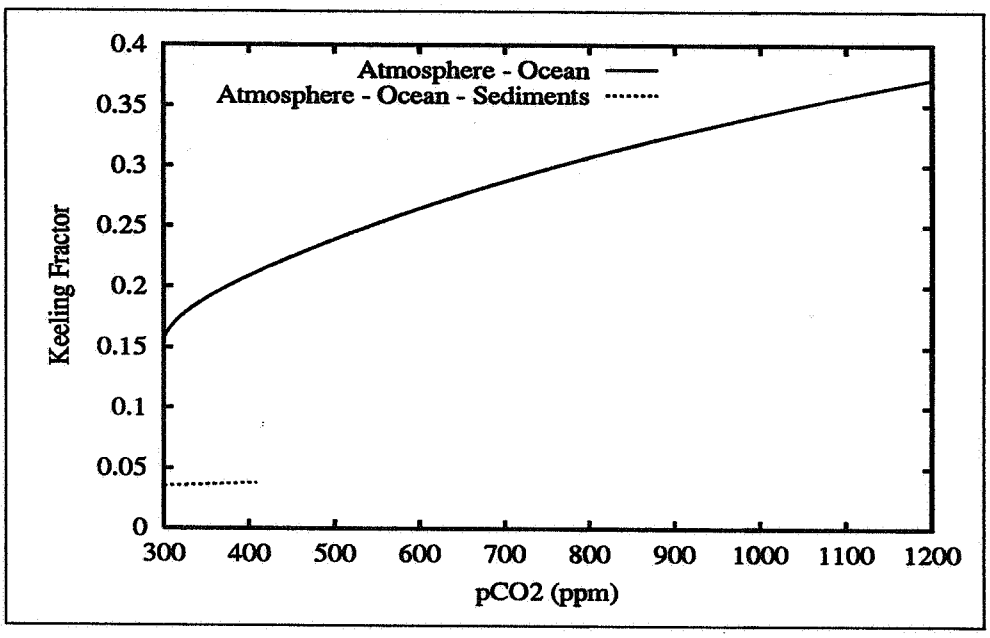

(a) The Keeling fraction f_K.

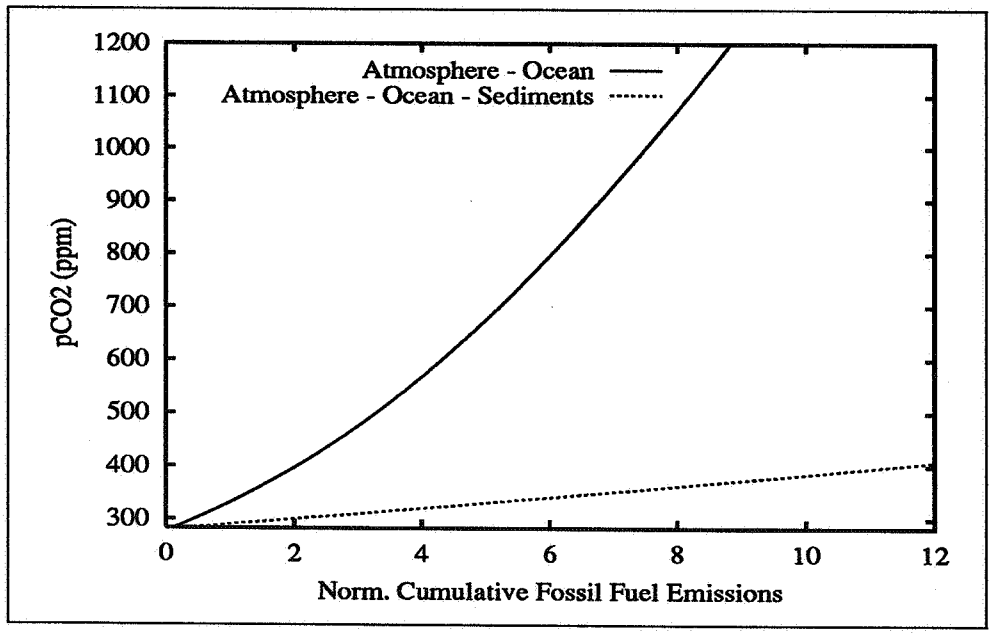

(b) The total amount of fossil fuel released since the industrial revolution, and the corresponding final atmospheric pCO_2 value.

Figure 25: The Keeling fraction and normalized cumulative fossil fuel emissions $M_{\rm ff}/M^0_{\rm atm}$ as functions of equilibrium pCO_2. The Atmosphere-Ocean curves represent equilibrium between the ocean waters and atmosphere, the Atmosphere-Ocean-Sediment curves represent equilibrium between the ocean waters, sediments and atmosphere. The latter curves end at $M_{\rm ff} = 12\,M^0_{\rm atm}$, a number which represents the recoverable fossil fuel reserve.

(see Tab. 10), we have that the alkalinity increases when sedimentary $CaCO_3$ dissolves. The assumption A = const. made in the previous calculation now becomes invalid. The sediment-curves are computed on the basis of the following simplifications: i) $[Ca^{2+}]$ = const and ii) $\delta C_t = \delta[HCO_3^-]$ (Broecker and Peng, 1982). The atmospheric equilibrium concentration is found to be about 410 ppm when the 7200 Gt C are burned.

The curves in Fig. 25 are based on simple, idealized models, and the information from the curves should be treated thereafter. Nevertheless, the Keeling fraction is expected to give an estimated picture of the atmospheric CO_2 content *when* a steady-state value is achieved, at least as long as the global carbon cycles remains, more or less, as it is today. Notice that the Keeling fraction says nothing about the evolution of the atmospheric CO_2 content, only the final steady-state value. This means that the pCO_2-values in Fig. 25 represent atmospheric steady-state values. Since equilibrium between the different reservoirs are determined by the global ocean circulation, such an equilibrium may be obtained after the order of thousand years. Notice also that it is impossible to reach the preindustrial atmospheric pCO_2 value *unless* substantial changes in the marine and terrestrial carbon cycles occur. Even with the $CaCO_3$ dissolution, there will be between 4 and 5% accumulation of the total emitted CO_2 in the atmosphere.

In the following paragraphs we compare the steady-state results reported in Sec.2 with the Keeling fraction.

A.2.1 Comparison With Hoffert *et al.*, 1979

Hoffert *et al.* released a total amount of 7090 Gt C, corresponding to 3330 ppm CO_2 if the released carbon had remained in the atmosphere. Their atmospheric steady-state value was 1150 ppm, or 26% of the released CO_2 was accumulated in the atmosphere. If we compare with Fig. 25, we find that a steady-state value of 1150 ppm gives $f_K \approx 0.36$, or a 36% accumulation. The agreement between the two models could have been better, but they certainly give the same order of magnitude of the final atmospheric CO_2 content.

Hoffert *et al.* assume that the effect of $CaCO_3$ dissolution would reduce the atmospheric pCO_2 by a factor two, i.e. to about 575 ppm, while Fig. 25(a) indicates a 5% accumulation, or a final value of about 450 ppm.

A.2.2 Comparison With Bacastow and Stegen, 1991; and Stegen *et al.*, 1991

Based on the Hamurg model, these authors found that a total injection of 0.1543 ppm CO_2, starting from an atmosphere with 282 ppm CO_2, would lead to an atmospheric accumulation value of 12%. This result is about the same as we would predict from Fig. 25(a).

A.2.3 Comparison With Maier-Reimer, 1991

For the Marchetti scenario (see Subsec. 2.3), Maier-Reimer give 15 and 7% as the airborne fraction of the released CO_2 without and with $CaCO_3$ dissolution, respectively. Maier-Reimer has run his model for only 110 years, and comparison with the Keeling fraction may be somewhat suspect; the 7% seems to be too high compared to the expected f_K value of 0.04. The discrepancy between the expected and reported fraction may be found in the short time of model integration: Since the exchange of CO_2 between the atmosphere and the ocean occurs through the uppermost well-mixed ocean layer, only a fraction of the absorbed CO_2 has reached the $CaCO_3$ sediments at the ocean bottom.

A.3 Inorganic Carbon Buffering in the Oceanic Surface Waters

The principal chemical reaction in seawater with repect to dissolved carbon dioxide is given by reaction (59):

$$H_2O + CO_2(aq) + CO_3^{2-} \rightleftharpoons 2HCO_3^- .$$

The uptake of atmospheric CO_2 occurs in the uppermost well mixed oceanic surface layer. In contrast to the previous subsection, the timescale for this uptake is 1 to 2 years, which is an estimate of the time required to transfer the CO_2 through the atmosphere ocean interface (Sec. 4) and to mix the uppermost 2–400 metres of the world ocean. Parts of the atmospheric CO_2 absorbed by the mixed layer will take part in the marine biology, or be transported into the deep ocean by vertical convection and sinking waters at high latitudes. The fate of the carbon by the latter process can only be estimated from numerical models. The nature of the surface water uptake, however, may be examined by means of the reactions and quantities given in Tab. 10.

From the above reaction, wee see that any increase in $[CO_2(aq)]$ leads to a reduction in the CO_3^{2-} concentration. There is a limited reservoir of CO_3^{2-}-ions available, so the question is: — How does the inorganic carbon buffering in the oceanic surface waters change with changes in the atmospheric pCO_2?

The answer of the above question may be found from the chemical properties of the factor $\partial C_T/\partial pCO_2$. If $\partial C_T/\partial pCO_2 > 0$, the surface layer absorbs parts of the atmospheric CO_2 as pCO_2 increases; and if $\partial C_T/\partial pCO_2$ is small, only a small fraction of the fossil fuel emissions will be absorbed by the oceanic surface layer.

As long as we consider the oceanic mixed layer, the alkalinity can be held constant. From the computations in the previous subsection, we know that C_T and pCO_2 may be written as functions of $[H^+]$, so

$$\left.\frac{\partial C_T}{\partial pCO_2}\right|_A = \left(\frac{\partial C_T}{\partial [H^+]} \Big/ \frac{\partial pCO_2}{\partial [H^+]}\right)_A . \tag{67}$$

In Eq. 67, the subscript A denotes that the alkalinity is held constant under differentiation. From the expression of the total inorganic carbon content C_T, Eq. 65, we have that

$$\frac{\partial C_T}{\partial [H^+]} = -pCO_2 \frac{K_0 K_1'}{[H^+]^2}\left(1 + 2\frac{K_2'}{[H^+]}\right) + K_0\left(1 + \frac{K_1'}{[H^+]} + \frac{K_1' K_2'}{[H^+]^2}\right) \left.\frac{\partial pCO_2}{\partial [H^+]}\right|_A . \tag{68}$$

The factor $\partial pCO_2/\partial[H^+]$ in the above expression can be found by using that the derivative of the alkalinity with respect to $[H^+]$ is zero. From Eq. 64, we then get

$$\left.\frac{\partial pCO_2}{\partial [H^+]}\right|_A = \frac{pCO_2}{[H^+]} \frac{[H^+] + 4K_2'}{[H^+] + 2K_2'} + \frac{[H^+]}{K_0 K_1'}\left(1 + 2\frac{K_2'}{[H^+]}\right)^{-1} \cdot \left\{ \frac{K_B' B_T}{([H^+] + K_B')^2} + \frac{K_w'}{[H^+]} + 1 \right\} . \tag{69}$$

In the following, we have set the alkalinity $A = 2.3$ meq kg^{-1}. The presented results are not sensitive to alkalinity values between 2.2 and 2.4 meq kg^{-1}, and this range in A acccounts for nearly all open ocean waters (Butler, 1982). $\partial C_T/\partial pCO_2$ is plotted in Fig. 26 as function of pCO_2. The curves in Fig. 26(a) show that the increase in the total inorganic carbon content of the oceanic surface waters decreases rapidly as pCO_2 increases. In fact, the reduction in $\partial C_T/\partial pCO_2$ is nearly 50% as pCO_2 increases from 300 to 500 ppm. This means that an increasing amount of the atmospheric fossil fuel emissions will remain in the atmosphere as pCO_2 increases.

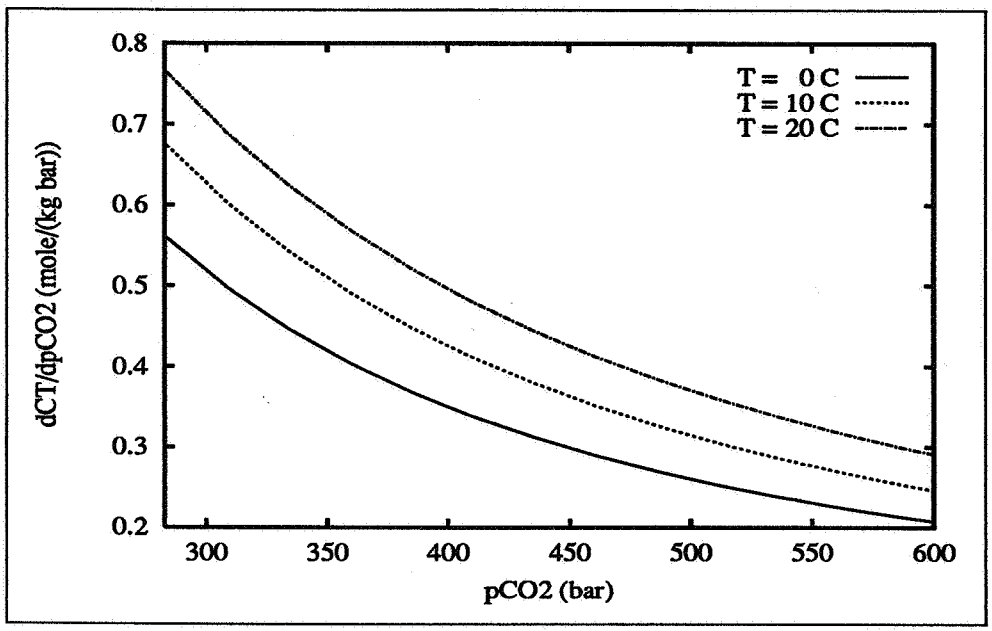

(a) $\partial C_T/\partial p\mathrm{CO}_2$ for $p\mathrm{CO}_2$ between 280 and 600 ppm.

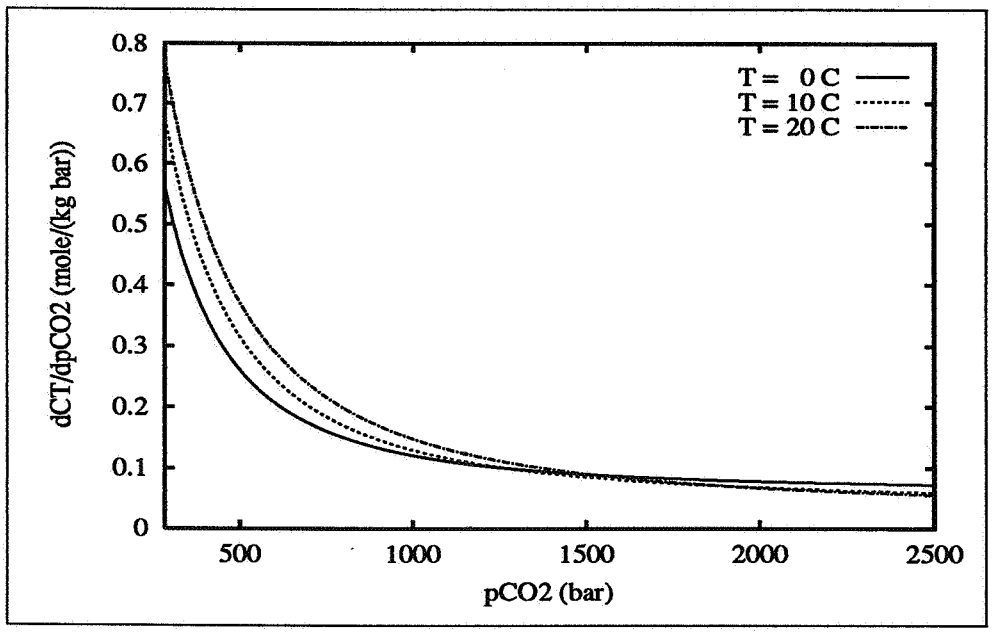

(b) $\partial C_T/\partial p\mathrm{CO}_2$ for $p\mathrm{CO}_2$ between 280 and 2500 ppm.

Figure 26: Inorganic carbon buffering in the oceanic surface waters. Curves computed from Eqs. 67–69, the apparent equilibrium constants are taken from UNESCO, 1987, $A = 2.3$ meq kg^{-1}, and $S = 35$ pro mil.

From Fig. 26(b), we see that the inorganic carbon content increases more in warm waters than in cold waters for $pCO_2 \lesssim 1500$ ppm. This might be somewhat surprising, since we know that the solubility of the CO_2 gas decreases quickly as the water temperature increases (see Fig. 9). If CO_2 had been an inert gas, the oceanic uptake of CO_2 would follow Henry's law, Eq. 22. We then would have that

$$\frac{\partial C_T}{\partial pCO_2} = \frac{\partial [CO_2(aq)]}{\partial pCO_2} = K_0 ,$$

where K_0 is Henry's law constant. For the temperatures 0, 10 and 20°C, the values of K_0 are 0.063, 0.044 and 0.032, respectively. From Fig. 26(b), wee see that the oceanic uptake of atmospheric CO_2 is approximately given by Henry's law as pCO_2 reaches 2500 ppm. This shows that the major uptake mechanism of atmospheric CO_2 for $pCO_2 \lesssim 1500$ ppm is not due to solubility of the CO_2 gas.

Substantial amounts of CO_2 enter the ocean for $pCO_2 \lesssim 1500$ ppm only because of reaction (59). That $\partial C_T/\partial pCO_2$ increases with temperature may be seen from a concentration diagram for $CO_2(aq)$, HCO_3^- and CO_3^{2-}, see Fig. 27. As we see, the concentration of CO_3^{2-} -

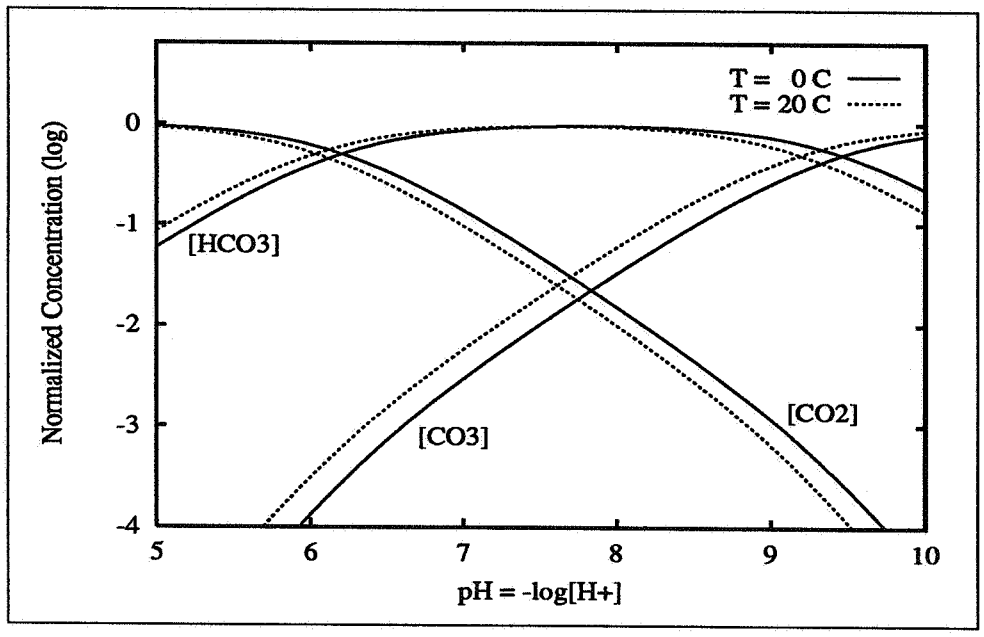

Figure 27: The shift in the inorganic carbon system with temperature for C_T = const.. Salinity $S = 35$ pro mil. Apparent equilibrium constants from UNESCO, 1987.

ions increases as the temperature increases. Thus, the temperature shift in the concentrations of the carbonic species results in more efficient buffering in warm waters than in cold waters.

That $\partial C_T/\partial pCO_2$ is larger for warm waters than cold waters does not mean that the warm waters are those which absorb most atmspheric CO_2. Fig. 28 shows $\partial C_T/\partial pCO_2$ for $280 \leq pCO_2 \leq 1000$ ppm as function of the total inorganic carbon content C_T, pCO_2 and temperature. This figure shows the features of Fig. 26, but also that cold waters contain more dissolved carbon than warm waters for a prescribed pCO_2 value.

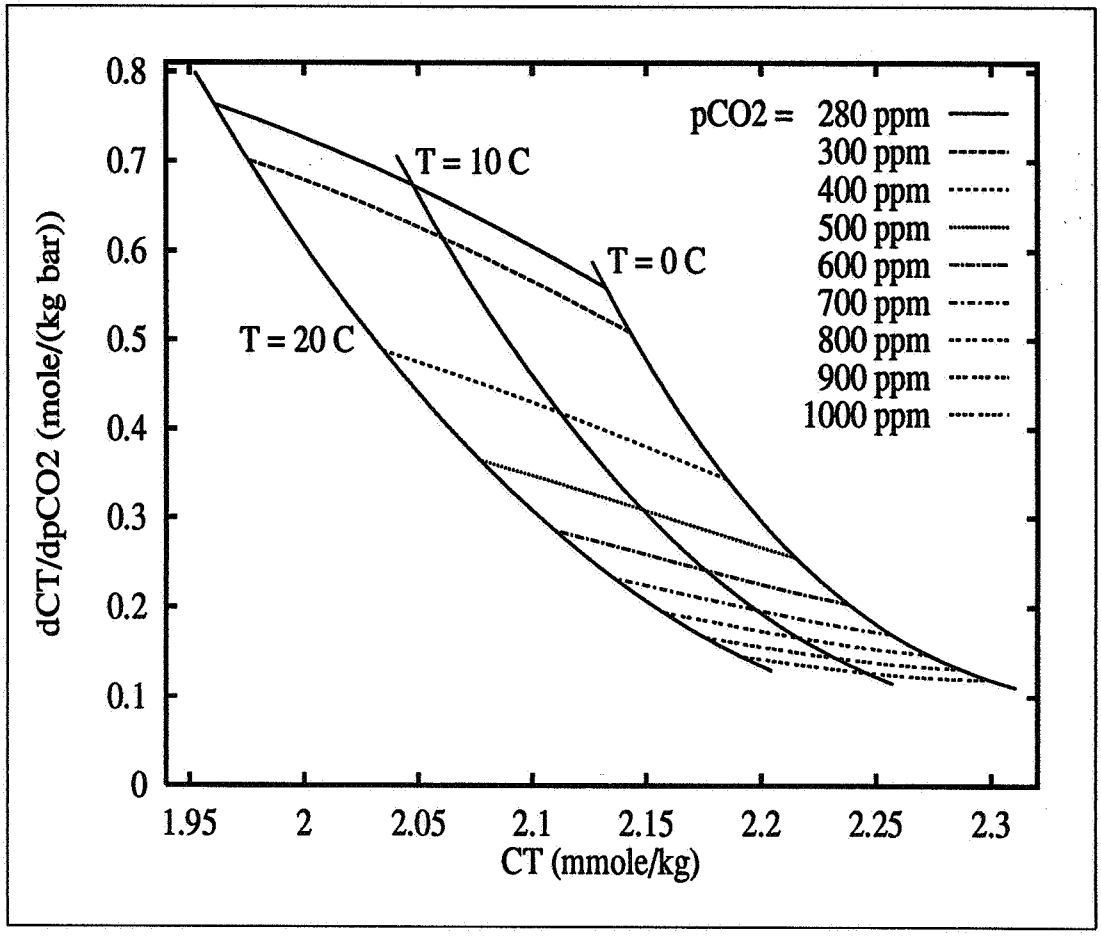

Figure 28: Change in $dC_T/dpCO_2$ as function of pCO_2, C_T and temperature. Alkalinity $A = 2.3$ meq kg^{-1}, salinity $S = 35$ pro mil. Computed from Eqs. 67–69, the apparent equilibrium constants are taken from UNESCO, 1987.

As a result of the present oceanic circulation pattern, there is a net uptake of atmospheric CO_2 in cold waters and outgassing in warm waters. Estimates of the net CO_2 flux at different pCO_2 levels therefore requires some model of oceanic transport. However, the fractional oceanic uptake of atmospheric CO_2 emissions will be reduced for any increase in atmospheric pCO_2.

A.3.1 Comparison With Maier-Reimer, 1991

Maier-Reimer reported that the Marchetti scenario was even more efficient than the direct effect of oceanic injection of one third of the total anthropogenic CO_2 'production' (Subsec. 2.3). This observation may be explained by the inorganic carbon buffering. Compared with conventional atmospheric emissions of fossil fuel CO_2, the oceanic uptake efficiency increases by keeping parts of the CO_2 away from the atmosphere and thus reduceing the C_T content of the oceanic surface layer. This is a general result which will apply to CO_2 which is disposed away from the atmosphere (Marchetti, 1989).

A.4 Summary

The ocean absorbs substantial amounts of the atmospheric CO_2 only because of the buffering reactions

$$H_2O + CO_2(aq) + CO_3^{2-} \rightleftharpoons 2HCO_3^-,$$

and

$$H_2O + CO_2(aq) + CaCO_3 \rightleftharpoons Ca^{2+} + 2HCO_3^-.$$

Although the oceanic waters and sediments have the capacity to neutralize the amount of carbon locked up in the fossil fuel reserves, only a certain fraction will be neutralized before a new equilibrium between the atmosphere, ocean and sediment reservoirs is achieved.

The fraction of emitted CO_2 which has been taken up by the oceans is presently 30–40% (Takahashi, 1989). On a very long time scale this fraction may increase to about 95%. With the present rates of increase in atmospheric pCO_2, the fraction is rapidly decreasing. Thus, reduced emissions to the atmosphere are required to maintain the strength of the oceanic sink. While injection in the ocean will not affect the final equilibrium between atmosphere, ocean and sediments, it may significantly reduce the transient maximum in atmospheric pCO_2.

References

Bacastow, R. and Maier-Reimer, E. (1991), Dissolved organic carbon in modelling oceanic new production, *Global Biogeochem. Cycles*, **5**:71–85.

Bacastow, R. and Stegen, G. R. (1991), Estimating the Potential for CO_2 Sequestration in the Ocean using a Carbon Cycle Model, *Oceanus*, **3**:1654–1657.

Baes, C. F., J., Beall, S. E., and Lee, D. W. (1980), The Collection, Disposal and Storage of Carbon Dioxide, in *Interactions of Energy and Climate*, edited by Bach, W. and Pankrath, J., pp. 495–519, Dordrecht, D. Reidel Publishing Company.

Batchelor, G. K. (1987), The stability of a large gas bubble rising through liquid, *J. Fluid Mech.*, **184**:399–422.

Bishnoi, P. R. and Robinson, D. B. (1971), An Evaluation of Methods for Determining the Parameters in the BWR Equation of State Using Volumetric and Heat Capacity Data, *Can. J. Chem. Eng.*, 49:642–650.

Bradshaw, A. (1973), The effect of carbon dioxide on the specific volume of seawater, *Limnol. Oceanogr.*, **18**:95–105.

Broecker, W. S. and Peng, T.-H. (1982), *Tracers in the Sea*, Lamont-Doherty Geological Observatory, Columbia University, New York 10964.

Butler, J. N. (1982), *Carbon Dioxide Equilibria and Their Applications*, Addison-Wesley, Reading, Mass.

Calderbank, P. H., Johnson, D. S. L., and Loudon, J. (1970), Mechanics and mass transfer of single bubbles in free rise through some Newtonian and non-Newtonian liquids, *Chem. Eng. Sc.*, **25**:235–256.

Cheney, W. and Kincaid, D. (1985), *Numerical Mathematics and Computing*, Brooks/Cole Publishing Company, Monterey, Calif.

Clift, R., Grace, J. R., and Weber, M. E. (1978), *Bubbles, Drops, and Particles*, Academic Press, New York.

Culcin, F. (1965), The major constituents of sea water, in *Chemical Oceanography*, edited by Riley, J. P. and Skirrow, G., pp. 121–161, London, Academic Press.

Etcheto, J., Boutin, J., and Merlivat, L. (1991), Seasonal variation in the air-sea CO_2 exchange coefficient over the global ocean using satellite wind speed measurements, *Tellus*, **43B**:247–255.

Gill, A. E. (1982), *Atmosphere-Ocean Dynamics*, Academic Press, San Diego.

Grace, J. R., Wairegi, T., and Brophy, J. (1978), Break-Up of Drops and Bubbles in Stagnant Media, *Can. J. Chem. Eng.*, **56**:3–8.

Haugan, P. M. and Drange, H. (1991), Effekt av CO_2-injeksjon i havet på det atmosfæriske CO_2-budsjettet, Technical Report 50, Nansen Environmantal and Remote Sensing Center, Bergen, In Norwegian.

Haugan, P. M. and Drange, H. (1992), Shallow Injection of CO_2: Efficient Sequestration in the Deep Ocean?, *Submitted to Nature*, -:-.

Haugan, P. M., Evensen, G., Johannessen, J. A., Johannessen, O. M., and Pettersson, L. H. (1991), Modeled and Observed Mesoscale Circulation and Wave-Current Refraction During the 1988 Norwegian Continental Shelf Experiment, *J. Geophys. Res.*, **96**:10487–10506.

Heinze, C., Maier-Reimer, E., and Winn, K. (1990), Glacial pCO_2 reduction by the world ocean-experiments with the Hamburg Carbon Cycle Model, Report 57, Max-Planck-Institut für Meteorologie, Hamburg.

Herzog, H., Golomb, D., and Zemba, S. (1991), Feasibility, Modelling and Economics of Sequestering Power Plant CO_2 Emissions in the Deep Ocean, *Envir. Prog.*, **10**:64–74.

Hoffert, M. I., Wey, Y.-C., Callegari, A. J., and Broecker, W. S. (1979), Atmospheric Response to Deep-Sea Injections of Fossil-Fuel Carbon Dioxide, *Climatic Change*, **2**:53–68.

Holt, T. and Lindeberg, E. (1990), Deponering av co_2 i verdenshavene og i ikke oljeførende geologiske formasjoner, Rapport til SFT, IKU, Trondheim, Norway, in Norwegian.

Killworth, P. D. (1977), Mixing on the Weddell Sea continental slope, *Deep Sea Res.*, **24**:427–448.

King, M. B. (1969), *Phase Equilibrium in Mixtures*, Pergamon Press, Oxford.

Kitscha, J. and Kocamustafaogullari, G. (1989), Breakup Criteria for Fluid Particles, *Int. J. Multiphase Flow*, **15**:573–588.

Kratz, G. (1985), Modelling the Global Carbon Cycle, in *The Handbook of Environmental Chemistry*, edited by Huntzinger, O., volume 1D, pp. 30–81, Berlin, Springer-Verlag.

Kritchevsky, I. R. and Iliinskaya, A. (1945), -, *Acta Physicochimika U.R.S.S.*, **20**:327–348.

Laider, K. J. and Meiser, J. H. (1982), *Physical Chemistry*, The Benjamin/Cummings Publ. Comp., Inc., Menlo Park, Cal.

Lee, D. W. (1980), An Analytical Model for a Vertical Buoyant Jet, Technical Report ORNL/TM–7140, Oak Ridge National Laboratory, Oak Ridge, Tennessee.

Lerman, A. (1979), *Geochemical Processes. Water and Sediment Environments*, John Wiley & Sons, New York.

Levine, I. N. (1988), *Physical Chemistry*, McGraw-Hill Book Comp., New York, 3 edition.

Maier-Reimer, E. (1991), Carbonate Buffering of anthropogenic CO_2, in *Strategies for Future Climate Research*, edited by Latif, M., pp. 319–339, Hamburg, Max-Plank-Institut für Meteorologie.

Maier-Reimer, E. and Bacastow, R. (1990), Modelling of geochemical tracers in the ocean, in *Climate-Ocean Interaction*, edited by Schlesinger, M. E., pp. 233–267, Kluwer Academic Publishers.

Maier-Reimer, E. and Hasselmann, K. (1987), Transport and storage of CO_2 in the ocean — an inorganic ocean-circulation carbon cycle model, *Climate Dynamics*, **2**:63–90.

Marchetti, C. (1977), On Geoengineering and the CO_2 Problem, *Climatic Change*, **1**:59–68.

Marchetti, C. (1989), How to solve the CO_2 problem without tears, *Int. J. Hydrogen Energy*, **14**:493–506.

Miller, S. L. (1974), The Nature and Occurrence of Clathrate Hydrates, in *Natural Gases in Marine Sediments*, edited by Kaplan, I. R., pp. 151–177, Plenum Press, New York.

Millero, F. J., Perron, G., and Desnoyers, J. E. (1973), Heat capacity of seawater solutions from 5 to 35°C and 0.5 to 22% chlorinity, *J. Geophys. Res.*, **78**:4499–4507.

Mitsubishi, J. K. K. (1990), Method for the fixation of carbon dioxide, apparatus for fixing and disposing carbon dioxide, and apparatus for the treatment of carbon dioxide, European Patent Application, Application Number: 90250288.9.

Mosby, H. (1977), De Nordiske Hav, in *Norges Geografi*, edited by Gjessing, J., pp. 143–154, Universitetsforlaget, In Norwegian.

Mustacchi, C., Armenante, P., and Cena, V. (1979), Carbon Dioxide Removal from Power Plant Exhausts, *Environment International*, **2**:453–456.

Riley, J. P. and Skirrow, G., editors (1975), *Chemical Oceanography*, volume I & II, Academic Press, London, 2nd edition.

Siegenthaler, U. (1983), Uptake of excess CO_2 by an Outcrop-Diffusion Model of the Ocean, *J. Geophys. Res.*, **88C**:3599–3608.

Smith, P. C. (1975), A streamtube model for bottom boundary currents in the ocean, *Deep Sea Res.*, **22**:853–873.

Stegen, G. R., Cole, K. H., and Bacastow, R. (1991), Sequestring of CO_2 in the Ocean, in *IEA International Conference on Technology Responses to Global Environmental Challenges*, Kyoto, Japan.

Stumm, W. and Morgan, J. J. (1981), *Aquatic Chemistry*, Wiley-Interscience, New York, 2 edition.

Takahashi, T. (1989), The carbon dioxide puzzle: Only half as much CO_2 as expected from industrial emissions is accumulated in the atmosphere. Could the oceans be the storehouse for the missing gas?, *Oceanus*, **32**:22–29.

Tse, F. C. and Sandall, O. C. (1979), Diffusion coefficients for oxygen and carbon dioxide in water at 25°C by unsteady state desorption from a quiescent liquid, *Chem. Eng. Commun.*, **3**:147–153.

Turner, J. S. (1973), *Buoyancy effects in fluids*, Cambridge Univ. Press, Cambridge.

Turner, J. S. (1981), Small-scale mixing processes, in *The Evolution of Physical Oceanography*, edited by Warren, B. A. and Wunsch, C., pp. 236–262, Cambridge, Mass., MIT Press.

UNESCO (1981), Tenth report of the joint panel on oceanographic tables and standards, Technical Papers in Marine Sci. 36, UNESCO, Paris.

UNESCO (1987), Thermodynamics of the carbon dioxide system in seawater, Technical Papers in

Marine Sci. 51, UNESCO, Paris.

Watanabe, H. and Iizuka, K. (1985), The Influence of Dissolved Gases on the Density of Water, *Metrologia*, **21**:19–26.

Weaset, R. C. and Selby, S. M., editors (1967), *CRC Handbook of Chemistry and Physics*, Cleveland, Ohio, The Chemical Rubber Co.

Weiss, R. F. (1974), Carbon dioxide water and seawater: The solubility of a non-ideal gas, *Mar. Chem.*, **2**:203–215.

Wilkinson, P. M. and v. Dierendonck, L. L. (1990), Pressure and gas density effects on bubble break-up and gas hold-up in bubble columns, *Chem. Eng. Sci.*, **45**:2309–2315.

Worthington, L. V. (1981), The Water Masses of the World Ocean: Some Results of a Fine-Scale Census, in *Evolution of Physocal Oceanography*, edited by Warren, B. A. and Wunsch, C., pp. 42–69, Cambridge, Mass., The MIT Press.